IRSTI 34.29.25; 68.37.31; 29.31.26 https://doi.org/10.26577/bb107220267

R.M. Ualiyeva[1*], A.V. Osipova[1], N.A. Diyanchuk[1],
M.M. Kaverina[1], S.B. Zhangazin[2], A.U. Tuyakbayeva[2]

[1]Toraighyrov University, Pavlodar, Kazakhstan
[2]L.N. Gumilyov Eurasian National University, Astana, Kazakhstan
*e-mail: ualiyeva.r@gmail.com

IDENTIFICATION OF BARLEY PHYTOPATHOLOGIES BASED ON SPECTRAL SIGNATURES OBTAINED VIA HYPERSPECTRAL IMAGING

This article investigates the hyperspectral characteristics of barley. A major challenge in agriculture is the inability to perform early disease diagnosis. Hyperspectral imaging enables the identification of diseases at an early stage, preventing their further spread. Spectral analysis of barley diseases (loose smut, leaf spot, root rot) shows that infected and dried tissues have low reflectance, early-stage infections exhibit medium reflectance, and healthy tissues display high spectral intensity. In hyperspectral images, diseased plant areas appear blue, areas with living but already infected tissue appear yellow, and healthy plant areas are shown in orange, red, and burgundy. Spectra from healthy areas possess high intensity compared to those from diseased zones. This is attributed to the presence of chlorophyll, the green pigment in healthy tissue that actively reflects light. The destruction of the epidermis, loss of moisture, tissue necrosis, and darkening lead to a decrease in reflected light intensity. Barley diseases like loose smut, rust, and root rot involve spores with melanin-like pigments. These cause the decay of healthy tissues, suppress photosynthetic activity, and absorb more light than they reflect. These diseases are identified by reduced reflectance in infected plant parts. In early leaf spot, chlorophyll degradation causes a yellow colour that may resemble healthy tissue. As metabolites accumulate and necrosis progresses, brown and dark spots develop. Consequently, this disease shows high spectral variability. Leaf spot can be differentiated by the non-uniform spectral intensity across different plant parts. A common feature of all phytopathologies is the overall reduction in the plant's reflectance. The obtained spectral profiles position hyperspectral imaging as a viable tool for monitoring barley agrocenoses. It enables differentiation of phytopathologies, detailed assessment of plant condition, and early detection of anomalies before visible symptoms appear. Further advances will enable targeted crop protection, lower pesticide costs, and reduce environmental impact.

Keywords: hyperspectral imaging, barley, phytopathology, plant diseases, spectra.

Р.М. Уалиева[1*], А.В. Осипова[1], Н.А. Диянчук[1],
М.М. Каверина[1], С.Б. Жангазин[2], А.У. Туякбаева[2]

[1]орайғыров университеті, Павлодар, Қазақстан
[2]Евразийский национальный университет им. Л.Н. Гумилева, Астана, Қазақстан
*e-mail: ualiyeva.r@gmail.com

Гиперспектралды визуализация арқылы алынған спектрлік сигнатуралар негізінде арпа фитопатологияларын идентификациялау

Бұл мақала арпаның гиперспектралды сипаттамаларын зерттеуге арналған. Ауыл шаруашылығының негізгі мәселелерінің бірі – ауруларды ерте диагностикалау мүмкіндігінің шектеулілігі. Гиперспектрлік бейнелеу ауруларды ерте кезеңде анықтауға және олардың одан әрі таралуының алдын алуға мүмкіндік береді. Шаңды қаракүйе, жапырақ дақтары және тамыр шірігі сияқты арпа ауруларының спектрлік сипаттамаларын зерттеу нәтижесінде аурумен зақымданған аймақтар мен қураған өсімдік ұлпаларының шағылу коэффициенті төмен, аурудың бастапқы кезеңдерінде орташа, ал сау ұлпаларда спектр қарқындылығы жоғары болатыны анықталды. Гиперспектралды кескінде өсімдіктің ауруға шалдыққан бөліктері көк түспен, тірі, бірақ жұқтырылған ұлпалар сары түспен, ал сау бөліктері қызғылт сары, қызыл және қоңыр-қызыл түстермен бейнеленеді. Сау аймақтардың спектрлері аурумен зақымданған аймақтардың спектрлерімен салыстырғанда жоғары қарқындылыққа ие. Бұл сау ұлпаларда жарықты белсенді түрде шағылдыратын жасыл пигмент – хлорофиллдің болуымен түсіндіріледі. Эпидермис құрылымының бұзылуы, ылғалдың жоғалуы, ұлпалардың некрозы және олардың қараюы

қындылығы төмендейді. Шаңды қаракүйе, тат және тамыр шірігі сияқты арпа аурулары сау ұлпалардың ыдырауына әкелетін, фотосинтетикалық жүйелердің белсенділігін төмендететін және шағылысқаннан гөрі көбірек жарық сіңіретін меланинтәрізді пигменттері бар споораларды қамтиды. Бұл ауруларды өсімдіктің зақымданған бөліктерінің шағылу коэффициентінің төмендеуі арқылы анықтауға болады. Жапырақ дақтарының бастапқы кезеңінде хлорофиллдің ыдырауы салдарынан ұлпалар сары түске ие болады, бұл оларды сау өсімдік ұлпаларымен шатастыруға әкелуі мүмкін. Метаболиттердің жиналуы және некроз процесі барысында қоңыр және қара түсті пигментті дақтар пайда болады. Осыған байланысты бұл ауру спектрлердің жоғары вариабельділігімен сипатталады. Дақ ауруын өсімдіктің әртүрлі бөліктеріндегі спектр қарқындылығының біркелкі еместігі арқылы ажыратуға болады. Барлық фитопатологияларға тән ортақ белгі – өсімдіктің жалпы шағылу қабілетінің төмендеуі. Алынған арпаның спектрлік профильдері гиперспектралды визуализацияны арпа агроценоздарын мониторингілеу әдісі ретінде қарастыруға мүмкіндік береді. Бұл тәсіл фитопатологияларды ажыратуға, егістіктің жағдайын жеке өсімдіктер деңгейінде егжей-тегжейлі талдауға және сыртқы белгілер байқалмай тұрып аномалияларды анықтауға жағдай жасайды. Осы саладағы болашақ зерттеулер қорғаныш құралдарын нысаналы түрде қолдануға, пестицидтерге жұмсалатын шығындарды азайтуға және қоршаған ортаға түсетін антропогендік жүктемені төмендетуге мүмкіндік береді.

Түйін сөздер: гиперспектралды визуализация, арпа, фитопатология, өсімдік аурулары, спектрлер.

Р.М. Уалиева[1*], А.В. Осипова[1], Н.А. Диянчук[1],
М.М. Каверина[1], С.Б. Жангазин[2], А.У. Туякбаева[2]

[1]Торайгыров университет, Павлодар, Казахстан
[2]Евразийский национальный университет им. Л.Н. Гумилева, Астана, Казахстан
*e-mail: ualiyeva.r@gmail.com

Идентификация фитопатологий ячменя по данным спектральных сигнатур, полученных с применением гиперспектральной визуализации

Данная статья посвящена изучению гиперспектральных характеристик ячменя. Одной из главных проблем сельского хозяйства является невозможность ранней диагностики заболеваний. Гиперспектральная визуализация позволит идентифицировать болезнь на ранних сроках и предотвратить ее дальнейшее распространение. Изучив спектральные характеристики таких болезней ячменя как пыльная головня, пятнистость, корневая гниль, было выявлено, что пораженные болезнью участки и высохшая растительная ткань имеют низкий коэффициент отражения, начальные стадии болезней – средний коэффициент отражения, а здоровая ткань обладает высокой интенсивностью спектра. На гиперспектральном изображении больные участки растения отображаются синим цветом, участки с еще живой тканью, но уже зараженные – желтым, а здоровые участки растений оранжевым, красным и бордовым. Спектры здоровых участков обладают высокой интенсивностью по сравнению со спектрами участков, пораженных болезнями. Это связано с тем, что здоровая ткань содержит зеленый пигмент хлорофилл, который активно отражает свет. При разрушении структуры эпидермиса, потере влаги, некрозе тканей и их потемнении интенсивность отражаемого света снижается. Болезни ячменя, такие как пыльная головня, ржавчина и корневая гниль, содержат споры с меланиноподобными пигментами, которые вызывают гниение здоровых тканей, угнетают активность фотосинтетических систем и поглощают больше света, чем отражают. Эти болезни можно идентифицировать по снижению коэффициента отражения зараженных участков растения. Пятнистость листьев на начальной стадии при разрушении хлорофилла имеет желтый цвет, который можно спутать со здоровой тканью растений. При накоплении метаболитов и некрозе появляются пигментные пятна бурового и темного цветов. За счет этого это заболевание имеет высокую вариабельность в спектрах. Дифференцировать пятнистость можно по неоднородности интенсивности спектров разных участков растения. Отличительной чертой всех фитопатологий является снижение общей отражательной способности растения. Полученные данные спектральных профилей ячменя позволяют рассматривать гиперспектральную визуализацию как метод мониторинга агроценозов ячменя, позволяющий дифференцировать фитопатологии, проводить детальный анализ состояния посевов на уровне отдельных растений и выявлять аномалии до проявления внешних симптомов. Дальнейшие разработки в этой области позволят точечно применять защитные средства, снизить затраты на пестициды и уменьшить нагрузки на окружающую среду.

Ключевые слова: гиперспектральная визуализация, ячмень, фитопатологии, болезни растений, спектры.

Introduction

Given the increasing intensification of agriculture and growing demands for sustainable agricultural production, the need to adopt high-precision methods for monitoring crop conditions is becoming evident. It is important to note that today, one of the most promising areas in digital agriculture is hyperspectral imaging – a technology based on recording the spectral characteristics of reflected radiation from vegetation across a broad range of wavelengths. Unlike traditional observation methods, hyperspectral imaging can detect physiological changes in plants at preclinical stages, which is particularly important as it plays a crucial role in enabling early diagnosis of diseases, nutrient deficiencies, and stress caused by unfavourable environmental conditions. Barley is one of the most important grain crops, sensitive to environmental changes and pathogen exposure, which directly affects yield and product quality.

Despite the proven effectiveness of this technology, a significant challenge in modern phytopathology is transitioning from isolated disease models to comprehensive diagnostic systems. While previous studies have successfully identified single-pathogen infections, there remains a critical need to accurately differentiate a complex of diverse diseases. Achieving this requires moving beyond standard vegetation indices to employ a deeper analysis of optical signatures, specifically utilising complex statistical parameters of spectral curves. Additionally, the physical relationship between specific disease manifestations – such as the accumulation of distinct fungal pigments – and their combined effect on the VNIR spectrum demands further investigation.

The object of this study is cultivated barley (*Hordeum vulgare* L.) grown in typical agroecological conditions of northeastern Kazakhstan. The subject of the research encompasses the specific optical signatures and hyperspectral reflectance parameters associated with healthy and pathogen-infected barley tissues. Therefore, our goal was to explore the potential of hyperspectral imaging in identifying barley diseases through the analysis of spectral profiles from infected plants. To achieve this aim, the following objectives were set: to acquire and pre-process hyperspectral data from healthy barley and samples infected with loose smut, plant rust, leaf spot, and root rot under controlled laboratory conditions; to calculate and analyse specific statistical indicators of reflectance; to extract informative spectral features and classify plant phytostatuses. To fulfill these objectives, the research employed hyperspectral imaging in the visible and near-infrared range. The analytical framework involved optical data acquisition followed by data dimensionality reduction and multivariate statistical processing to evaluate the spectral differences between the samples.

The scientific significance of this study lies in establishing quantitative links between physiological plant degradation (such as chlorophyll loss or melanin-related darkening) and specific variations in hyperspectral profiles. Practically, the proposed multidimensional evaluation offers detailed physiological insights that can inform the future development of automated monitoring systems, thereby contributing to more targeted agrochemical applications in precision agriculture.

The application of hyperspectral imaging in phytopathology has been the subject of extensive recent research, demonstrating significant potential for non-invasive crop monitoring. Recent studies have made substantial scientific contributions by validating the efficacy of spectral analysis for both early pathogen detection and the visualisation of plant resistance responses. These works highlight a vital transition in digital agriculture from traditional visual assessment to automated, high-precision phenotyping.

For instance, one study developed a highly accurate automated hyperspectral phenotyping system to quantitatively assess the severity of powdery mildew infection on different barley varieties under greenhouse conditions. This system successfully detected disease symptoms at early stages while achieving high classification accuracy without expert involvement (Thomas et al., 2018). It is worth noting that modern hyperspectral imaging methods, combined with principal component analysis, spectral decomposition, and linear discriminant analysis, enable high accuracy in the early detection of *Magnaporthe oryzae* infections on barley leaves and allow visualisation of infection sites as early as 24 hours after inoculation (Zhou et al., 2019). Additionally, it has been found that near-infrared hyperspectral imaging can accurately detect fungal infections by *Aspergillus glaucus* and *Penicillium spp.*, as well as ochratoxin A contamination in barley grains, thereby enabling early diagnosis and quality control of stored grain

(Senthilkumar et al., 2016). Hyperspectral imaging has demonstrated its practical effectiveness in the early detection of barley's hypersensitive response to *Blumeria graminis f. sp. hordei*, allowing for the identification of genotype-specific spectral signatures within 1-3 days after infection. This makes the method promising for automated phenotyping of disease resistance (Kuska et al., 2017). Overall, the practical application of hyperspectral imaging has enabled non-invasive detection and visualisation of barley resistance responses to *Blumeria graminis f. sp. hordei*, encompassing both pathogenesis and the manifestation of early hypersensitive reactions, even before visible symptoms appear. The use of the Relief algorithm, alongside parallel molecular-histological analysis, plays an equally important role by helping interpret spectral data in a biological context and identifying key wavelengths associated with different types of interaction (Kuska, 2017). Studies in this field also indicate that early detection of barley diseases using fluorescence and reflectance spectral indices effectively identifies diseases at initial stages and assesses chlorophyll concentration in leaves, facilitating timely fungicide application and improved crop management (Yu et al., 2014). Some research demonstrates that hyperspectral imaging has also been applied to non-destructive analysis of deoxynivalenol (DON) content in barley grain caused by *Fusarium graminearum* infection. Furthermore, data show that using partial least squares and machine learning methods enables high accuracy in estimating mycotoxin content, making this approach promising for rapid grain quality screening and Fusarium head blight diagnosis (Su et al., 2021). Hyperspectral imaging in the UV range allows for distinguishing between barley variaties resistant and susceptible to *Blumeria graminis f. sp. hordei* at early stages by detecting changes in reflectance, which may be related to flavonoids and other metabolites (Brugger et al., 2021). Hyperspectral imaging at a microscopic scale enables non-invasive recording of spectral changes in barley leaves during interaction with powdery mildew, helping differentiate susceptible and resistant genotypes based on reflectance in the visible and near-infrared ranges. In addition to these methods, automated analysis techniques such as Simplex Volume Maximisation (SiVM) contribute to faster data processing and yield clear results (Kuska et al., 2015). Equally important is the combined analysis of hyperspectral reflectance and transmission, which not only allows detection of barley powdery mildew before visual symptoms appear but also clarifies the spatial distribution of infected and necrotic areas. This makes the approach particularly valuable for early diagnosis and detailed pathogenesis studies (Thomas et al., 2016).

Despite these significant advancements, a critical research gap remains. The majority of the reviewed studies focus primarily on single-pathogen interactions or rely on standard evaluation methods without fully exploring the comprehensive statistical parameters of the spectral curves. There is a clear need for comparative research that simultaneously differentiates a complex of distinct phytopathological conditions – such as loose smut, plant rust, leaf spot, and root rot – based on detailed statistical reflectance metrics, including spectral bandwidth broadening and skewness shifts. Furthermore, there is limited quantitative exploration regarding how specific pathogen-induced alterations, particularly the accumulation of melanin-like pigments, simultaneously affect visible and near-infrared reflectance across different diseases. By providing a multidimensional statistical evaluation of hyperspectral data under controlled laboratory conditions, this study aims to differentiate diverse barley diseases, offering detailed spectral insights that can support the future development of remote monitoring systems in precision agriculture.

Materials and methods

The object of the study is cultivated barley (*Hordeum vulgare L.*) grown in the typical agroecological conditions of northeastern Kazakhstan. The collection of samples was carried out during key phenological stages of spring barley in 2025 in the main grain-producing districts of the Pavlodar region: Zhelezinka and Terenkol districts. These regions were selected based on their agricultural significance and differences in soil and climatic conditions, which ensured the sample's representativeness and allowed for capturing a wide range of possible plant phytosanitary conditions. Phytopathogens were diagnosed using laboratory methods (pure culture isolation, microscopy) in accordance with State Standard 12044-93 "Methods for Determining Disease Contamination" (State Standard 12044-93, 2011). Hyperspectral imaging of the plant material was conducted at the Biological

Research Laboratory of the Toraighyrov University. A high-precision FigSpec FS-13 hyperspectral camera, operating in the visible and near-infrared range (VNIR, 400-1000 nm), was used as the measuring instrument. This push-broom scanning camera features high spectral resolution (at least 2.5 nm) and a wide number of spectral channels (at least 250), enabling the acquisition of detailed spectral profiles of the studied objects. The imaging procedure was based on several key steps, including system calibration using reference white and black panels to ensure the correctness of reflectance data. Hyperspectral images were obtained under controlled lighting conditions to minimise the influence of external factors. For the preliminary assessment of data quality, specialised Breeze software, developed in the IDL (Interactive Data Language) programming environment, was used to visualise spectral cubes and perform their initial analysis. To identify signs of barley phytopathological conditions, the spectral data underwent comprehensive analytical processing.

A total of 17 barley samples representing different phytosanitary conditions were included in the study. The dataset consisted of one healthy sample, five samples infected with loose smut, five samples exhibiting symptoms of leaf spot diseases, two samples affected by rust, three samples with root rot, and one sample showing a mixed infection of loose smut and rust. Regions of interest corresponding to healthy and diseased plant tissues were selected from the hyperspectral images. On average, 8-10 ROIs were identified per image, resulting in approximately 150 ROIs across the entire dataset. Each ROI contained numerous spectral pixels with reflectance values recorded across the investigated spectral range. In total, approximately 50,000 spectral pixels were analysed and used for the calculation of spectral characteristics, Principal Component Analysis (PCA), and subsequent statistical processing.

The analysis of reflectance spectra was aimed at identifying characteristic spectral features – primarily zones of selective absorption and reflectance of radiation – which are presumably associated with physiological changes in plant tissues caused by diseases. These optical signatures were considered key markers for identifying different types of damage. An important stage in hyperspectral analysis is data dimensionality reduction and the extraction of informative spectral features. For this purpose, PCA method was applied. It allowed for structuring the spectral data, visualising them as projections onto new orthogonal axes, and conducting subsequent classification of plant phytosanitary status. The proposed methodological approach ensured high accuracy in distinguishing between healthy and diseased plants. Consequently, it may serve as a basis for the development of remote monitoring systems and early disease diagnosis in agroecosystems.

For statistical analysis with support for the Python programming language integrated with Microsoft Excel for more convenient data import and analysis. Spectral data were analysed using analysis of variance (ANOVA) along with descriptive statistical methods.

Minimum and Maximum Reflectance (Ualiyeva et al., 2025):

$$R_{min} = \min(R_1, R_2, \dots, R_n)$$

$$R_{max} = \max(R_1, R_2, \dots, R_n).$$

Mean Reflectance (Ualiyeva et al., 2025):

$$\mu = \frac{1}{n}\sum_{i=1}^{n} R_i.$$

Standard Deviation (dispersion of reflectance values) (Ualiyeva et al., 2025):

$$\sigma = \sqrt{\frac{1}{n}\sum_{i=1}^{n}(R_i - \mu)^2}.$$

Coefficient of Variation (degree of variability) (Ualiyeva et al., 2025):

$$CV = \frac{\sigma}{\mu} \times 100.$$

Delta Reflectance (difference) (Ualiyeva et al., 2025):

$$\Delta R = R_{max} - R_{min}.$$

Spectral Bandwidth calculated using the formula (Ualiyeva et al., 2025):

$$SB = \lambda_{max} - \lambda_{min}.$$

Spectral Skewness (asymmetry) (Ualiyeva et al., 2025):

$$SA = \frac{1}{n}\sum_{i=1}^{n}\left(\frac{R_i - \mu}{\sigma}\right)^3.$$

The computed parameters offer a quantitative evaluation of the spectral properties of the examined specimens and facilitate the identification of intergroup differences.

Results and discussion

The images with the spectral characteristics of barley feature graphs of the Raw Spectrum showing spectra from individual plant parts or overall spectra for each sample, a Variance Scatter diagram, and a hyperspectral image of the object. The Variance Scatter diagram in the center of the lower part of the image shows the distribution of spectral points according to Principal Component Analysis (PCA) components, with axis labels t[1] – the first principal component (major contributor to variance), and t[2] – the second principal component.

Healthy sample

On the left side of the presented image with healthy barley, the curves of spectra belonging to different parts of the plant are sequentially marked. For example, the first spectrum, represented by the red curve, belongs to the entire plant. Figure 1 shows healthy barley.

Figure 1
Healthy sample

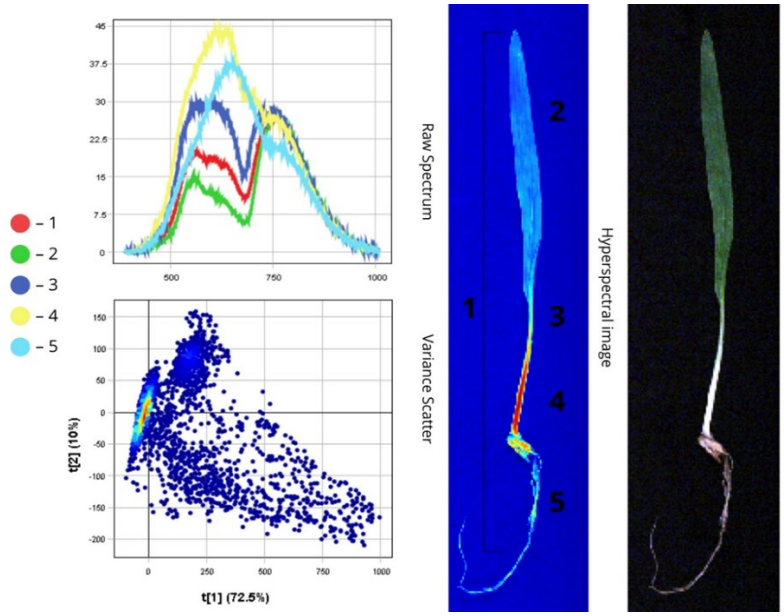

Note: Compiled by the author

The red curve represents the spectrum of the entire plant, featuring two peaks at wavelengths of 550 nm and 750 nm with a reflectance coefficient of 20-30. The leaf blade (green curve) represents a spectral peak at 550 nm with a reflectance coefficient of 15-20. The stem has a reflectance coefficient of 30 and spectral peaks at wavelengths of 550 nm and 750 nm. The coleoptile has the highest spectral intensity with a reflectance coefficient of 45 and a spectral peak at 550-600 nm. The root part has a reflectance coefficient of 37.5 and a spectral peak at 600 nm. At the same time the white coleoptile and root part have greater spectral intensity compared to the dark green leaf blade and stem.

Diseased Samples

Figure 2 presents samples of plants infected by various disease pathogens.

Figure 2
Diseased samples

Note: Compiled by the author

On each image depicting plant diseases, the legend is shown on the right: for example, the blue colour in the hyperspectral image corresponds to the red curve on the spectrum. It is very important to pay attention to this and not confuse the colours on the hyperspectral image and on the spectral graphs.

Loose smut

Loose smut is a disease of cereal crops caused by basidiomycete smut fungi, where infection occurs through teliospores. This infection typically manifests as disintegrating plant tissue from which a dusty black mass is formed. The spores can overwinter on plant residues and in soil, gradually transferring to young plants in spring and infecting them.

Figure 3 shows a stem and ear infected with loose smut. Graph 1 displays the spectral characteristics of the stem parts. Here, the red spectrum on the graph corresponds to the blue areas on the stem, and the green spectrum corresponds to the light blue areas, both of which are affected by loose smut. They are characterised by low spectral intensity with a reflectance coefficient of 10-30. On the other hand, the remaining spectra belong to unaffected plant tissue and have a higher reflectance coefficient, while the ear exhibits similar spectral characteristics. Important attention should be paid to the healthy plant tissue, which is depicted in burgundy and red on the hyperspectral image. The spectral graphs in purple, light blue, and blue colours show the highest reflectance intensity – 50-70. It was also found that the red spectrum corresponds to areas of the ear infected with loose smut and has the lowest reflectance coefficient – around 10. Examining the graph of the overall plant spectra revealed that these spectra have a low reflectance coefficient (15) due to the plant's infection, with the reflectance peak occurring at wavelengths within 500-780 nm. The Variance Scatter diagram deserves special attention, where the first principal component t[1], explaining 93.7% of the total variance, is the primary and most important axis along which the greatest data diversity lies. Meanwhile, the second component t[2], explaining 2.63% of the variance, reflects less significant variations. As a result, the plotted points form an elongated, slightly fan-shaped structure, which indicates the presence of two main types of spectra that vary between each other. Thus, it shows that the main difference between the spectra of objects 1 and 2 lies in the intensity and shape of the spectral curve.

Figure 3
Sample A: Loose smut

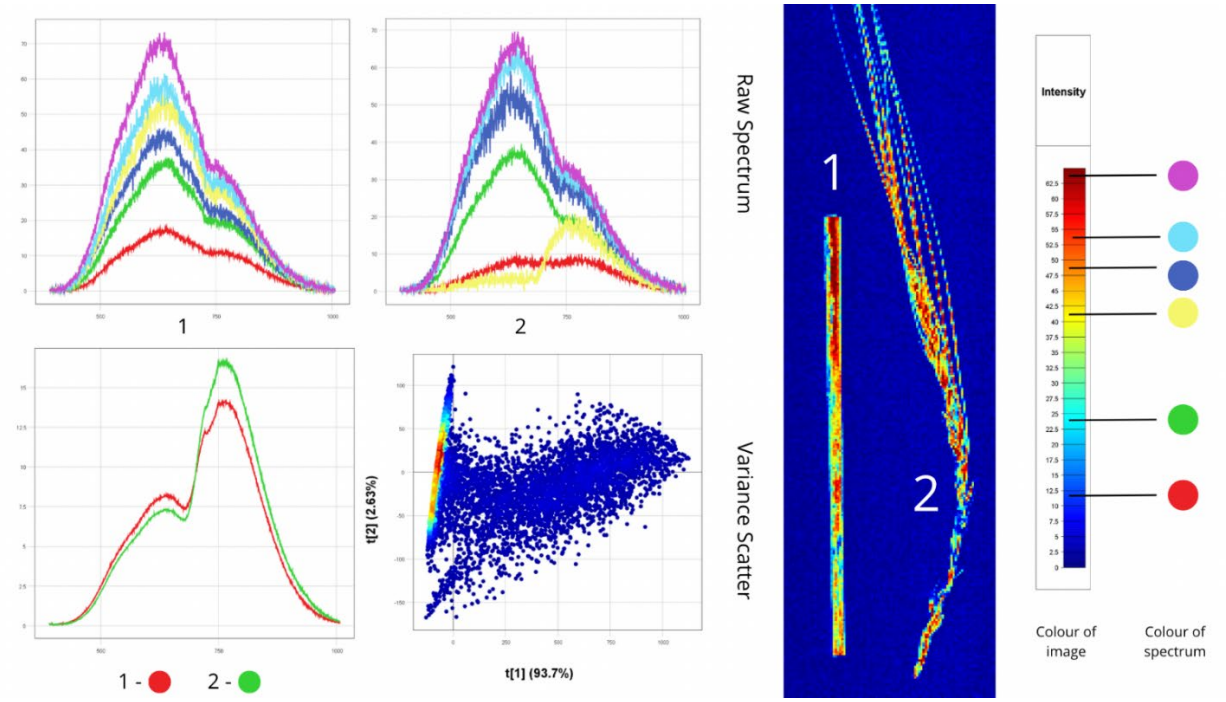

Note: Compiled by the author

Figure 4 shows images of barley leaves with a stem infected with loose smut. Graph 1 belongs to the first sample – a barley leaf that is completely infected with the disease. In the hyperspectral image, areas with the disease are shown in blue and light blue, while an area with progressing disease is shown in yellow. The study found that the red spectrum corresponds to the infected area and has a low reflectance coefficient of 15. The blue spectrum in this case belongs to an area with progressing loose smut but still-living plant tissue and has a medium reflectance coefficient of 45. The same trend is observed for the other samples: areas completely infected with loose smut are shown in blue and have the lowest reflectance, while the remaining healthy areas, for example in the third sample, are shown in red and have the highest intensity among the other spectra. Since the first sample is completely infected, it has the lowest reflectance among the other plants – 7.5, as seen in the overall graph. The third sample, in turn, has remnants of unaffected plant tissue, so its reflectance coefficient is the highest among the others – 17.5, with the reflectance peak occurring at a wavelength of 500-780 nm.

In the first sample of Figure 5, the stem is infected with loose smut, and the spectrum of the infected area has the lowest reflectance. The second sample has diffuse lesions on the stem, and the leaf and ear are completely infected. It was determined that the diffuse lesions are coloured yellow in the hyperspectral image, the leaf and ear are blue, while healthy tissue is coloured red and has a spectrum with the highest reflectance peak – 70. The third and fourth samples have pronounced disease on the ear, where the reflectance coefficient of the infected areas is 10. Among all samples, the first sample has the lowest overall reflectance coefficient as it contains the least amount of healthy tissue, and the reflectance peak lies within the wavelength range of 500-780 nm.

Figure 4
Sample B: Loose smut

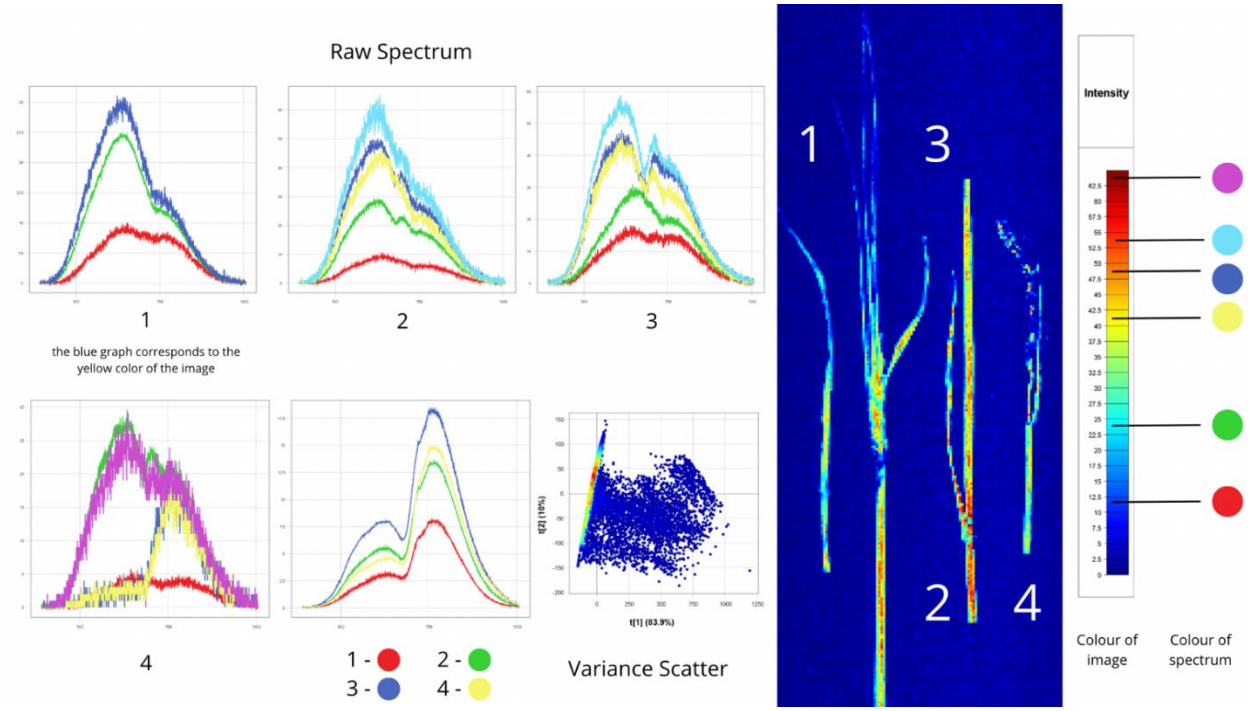

Note: Compiled by the author

Figure 6 shows a barley stem and ear partially infected with loose smut, where the green and red spectra belong to the infected plant areas. From the presented hyperspectral image, it is clear from the overall graph that the stem spectrum shows more pronounced disease symptoms than the ear spectrum, as it has lower reflectance intensity. The reflectance peak is also recorded within the wavelength range of 500-750 nm.

Figure 7 shows ear samples infected with loose smut. The first sample has a greater degree of infection and contains almost no areas coloured red, while the second sample contains more healthy tissue with a reflectance coefficient of 80. The results indicate that in the overall graph, the first sample has lower reflectance intensity – 11, compared to the second sample – 17.

Figure 5
Sample D: Loose smut

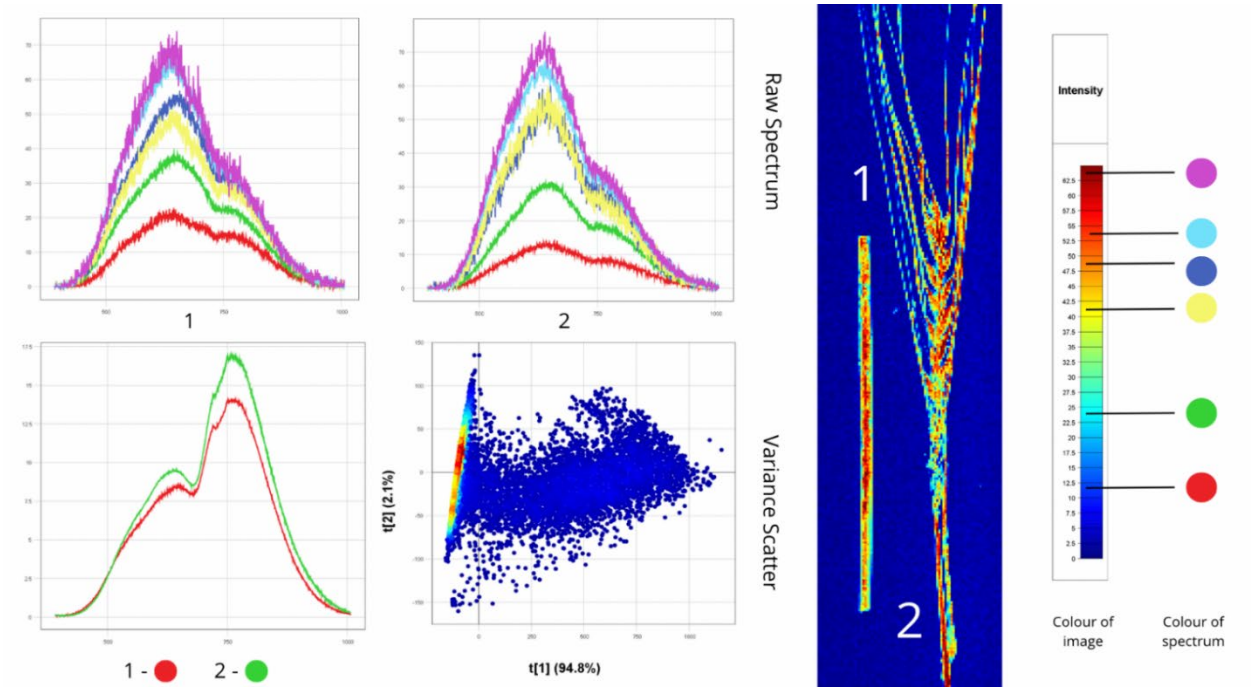

Note: Compiled by the author

Figure 6
Sample C: Loose smut

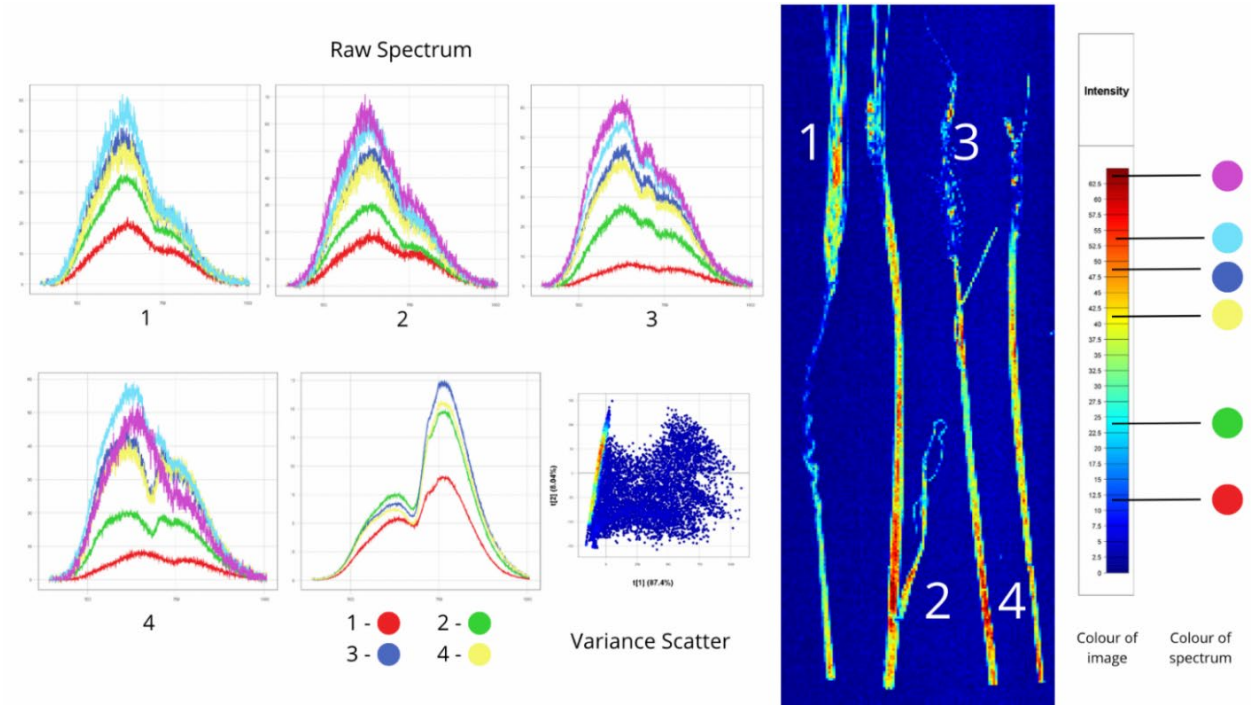

Note: Compiled by the author

Figure 7
Sample E: Loose smut

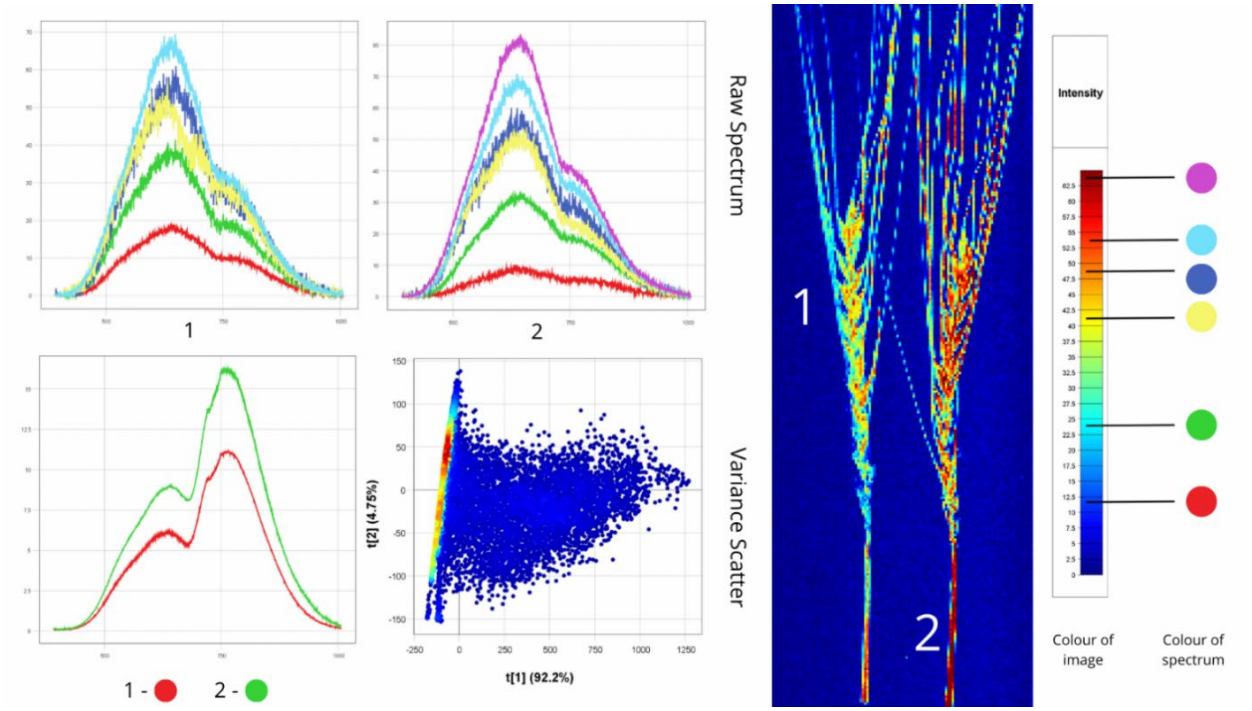

Note: Compiled by the author

Loose smut and plant rust

Figure 8 shows samples where barley stems are affected by loose smut and rust. In contrast to loose smut, rust appears as separate orange or brownish spots. In the hyperspectral image, the first and third samples are affected by loose smut, identifiable by the uniform distribution of blue and light blue colours. The second sample is affected by rust, the presence of which can be determined by the separately located areas of blue and light blue colour along the entire plant stem. The obtained results show that the spectra in terms of reflectance intensity for both diseases are approximately equal and recorded at a level of 10. It is also important to note that in the overall graph, the first sample has the lowest reflectance coefficient, as it is completely affected by loose smut, while the second and third samples retain some areas of healthy tissue.

Plant rust

Figure 9 shows barley stems affected by rust. The results indicate that in the hyperspectral image, rust can be identified by dark blue spots along the stems of all four samples. For example, in the first sample on the hyperspectral image, light blue and blue colours are pronounced, indicating that the entire stem is affected by rust. The analysis of the Raw Spectrum graph also shows that light blue areas have medium intensity, while blue ones have lower intensity. It was found that sample 4 is the most saturated in terms of spectral diversity, containing both diseased areas and healthy tissue. The overall spectral graph displays the general spectra of the barley stem samples, from which it follows that the third and fourth graphs have approximately similar reflectance values with a peak at 19. The reflectance peak of the first sample demonstrates the lowest reflectance coefficient numerically – 11, indicating that it is the most infected with rust among all samples. In objective terms, the Variance Scatter diagram is constructed based on component analysis: the axes represent the values of t[1] (91%) and t[2] (4.65%). The obtained results, showing a dense clustering of points, indicate a certain homogeneity between the spectra. Consequently, the resulting blurring along t[1] suggests significant differences between the areas (healthy and diseased), which is particularly clearly traced in the range of the main component, considered the most informative.

Figure 8
Sample F: Loose smut and plant rust

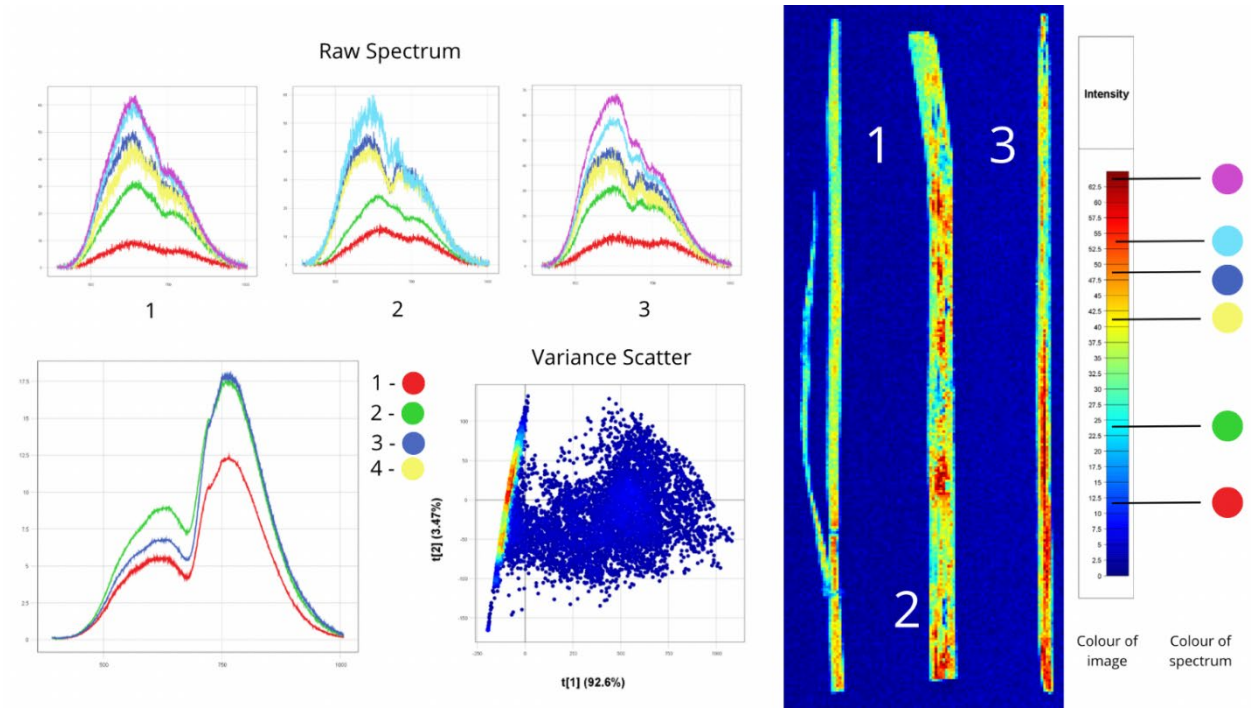

Note: Compiled by the author

Figure 9
Sample H: Plant rust

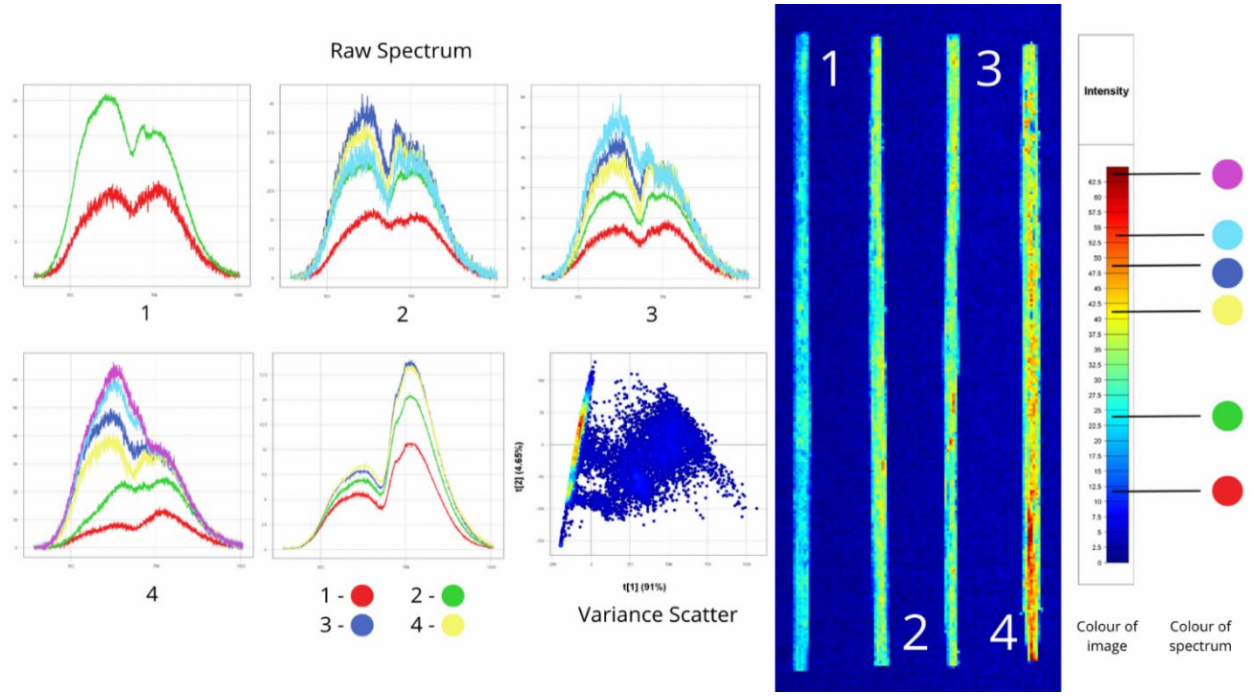

Note: Compiled by the author

Figure 10 depicts rust on a barley stem. This obtained hyperspectral image shows the intensity of reflected light in various areas of the stem, where zones of blue and light blue colours, corresponding to infection sites, are highlighted.

It was established that they have low reflectance intensity – 20, while healthy areas have a reflectance coefficient of 50. The analysis of the overall Raw Spectrum graph shows an averaged spectrum with two pronounced reflectance peaks – one is evident in the 550 nm region and a more pronounced peak recorded approximately in the range around 750 nm. These results are explained by chlorophyll actively absorbing light in the red zone and reflecting it in the near-infrared. Examining the issue of dispersion intensity, it becomes clear that the Variance Scatter diagram shows a strong separation along the t[1] axis, which explains over 92% of the total variance. This indicates the presence of clear differences between spectral subgroups, specifically between healthy and diseased tissues. Since the high density of points on the left and the scattered cloud on the right collectively emphasise that the spectral data of the stem is not homogeneous, this can be directly related to the visually and spectrally distinguishable foci of rust.

Figure 10
Sample P: Plant rust

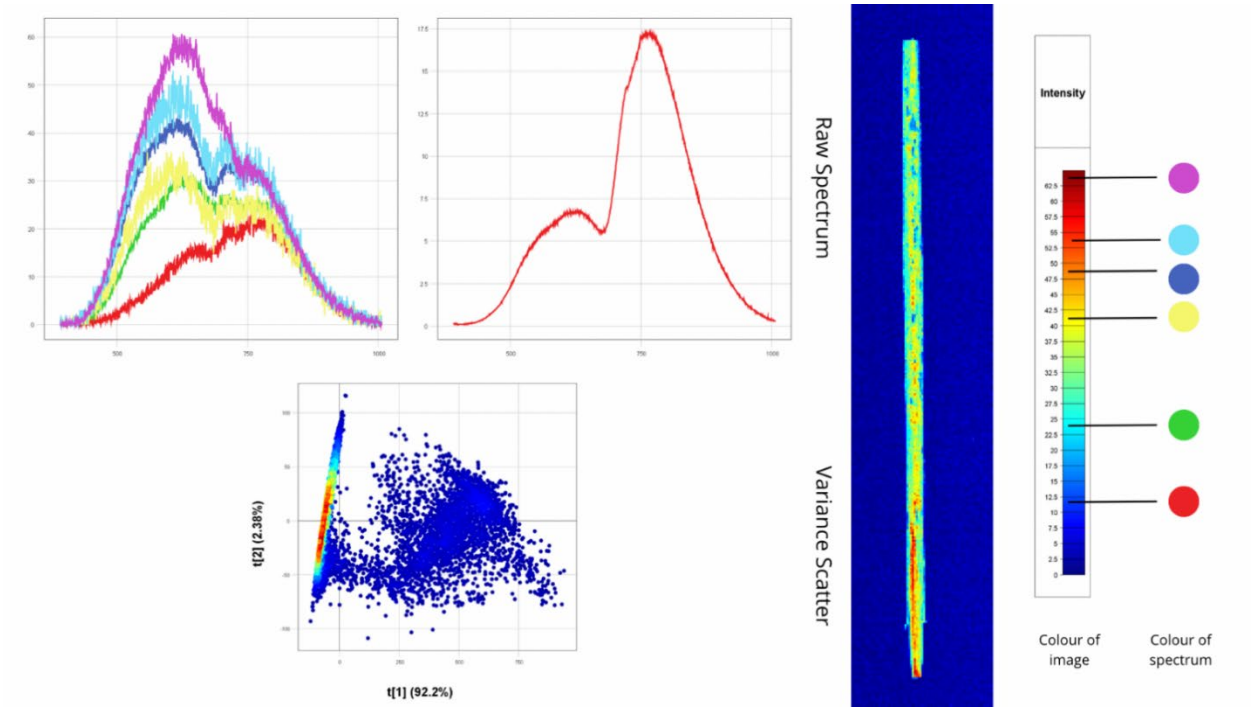

Note: Compiled by the author

Leaf spot

Figure 11 shows barley leaves affected by leaf spot, which appears as yellow and turquoise colours in the hyperspectral image and is mainly observed at the leaf tips, making it potentially mistaken for healthy tissue. However, blue dots are also visible in these areas, indicating the presence of leaf necrosis. Overall, an objective analysis of the Variance Scatter diagram demonstrates that leaf spot causes significant spectral differences, resulting in clusters with reduced reflectance that are spatially separated from healthy tissues.

Figure 11
Sample G: Leaf spot

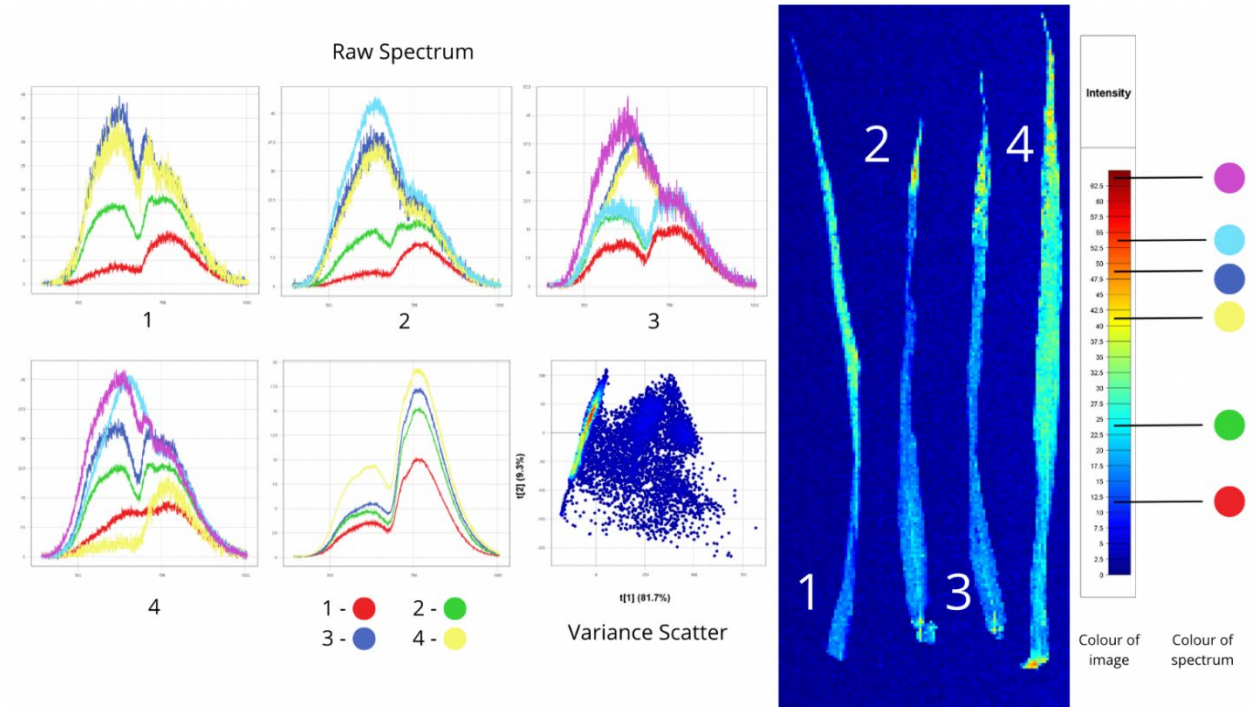

Note: Compiled by the author

Figure 12 depicts a barley leaf with leaf spot. In the hyperspectral image, necrosis is visualised as dark blue spots spread along the entire length of the sample, particularly noticeable at the edges. Red and yellow areas show high reflectance intensity, characteristic of healthy leaf cells, while on the Raw Spectrum graph, the peak of the dark blue spectrum is at 18. In turn, the spectra of light blue, yellow, orange, red, and dark red colours correspond to areas with less damage. As the intensity increases (to dark red), a rise in reflectance peaks is observed, especially in the 700-800 nm range. An important aspect is the consideration of dispersion on the Variance Scatter graph, which presents Principal Component Analysis (PCA): the t[1] axis (81.5%) represents the main component explaining most of the data variability, while the t[2] axis (5.8%) represents the second component, complementing the analysis. The visualisation of points on the graph corresponds to spectra from different image pixels, where a strong aggregation of points is observed on the left along the t[1] axis, but some points significantly deviate to the right, which may correspond to necrotic areas with a distinctly different spectrum. It was also established that the obvious presence of a colour gradient in the points (from red to blue) emphasises the degree of spectral alteration, where red likely highlights tissues with the greatest degree of damage.

Figure 13 presents a hyperspectral image of a barley leaf affected by leaf spot. This image clearly shows necrotic areas displayed as dark blue dots with low reflectance intensity, particularly at the upper tip of the leaf. There are also light yellow areas indicating medium reflectance, characteristic of the initial stages of leaf spot. The graph with a single curve shows the averaged leaf spectrum and demonstrates a pronounced peak in the range from 600 nm to 780 nm, with a reflectance coefficient equivalent to 17.5, which is presumably characteristic of a diseased plant. The overall spectral graph displays numerous spectra corresponding to different leaf zones, with colours comparable to those in the hyperspectral image. On the Variance Scatter graph obtained by Principal Component Analysis (PCA), the t[1] axis (87.9%) represents the main direction of spectral variability, while the t[2] axis (3.28%) complements the analysis. It follows that the distribution of points shows a compact clustering on the left, while a scattered cloud of points is observed further to the right.

Figure 12
Sample I: Leaf spot

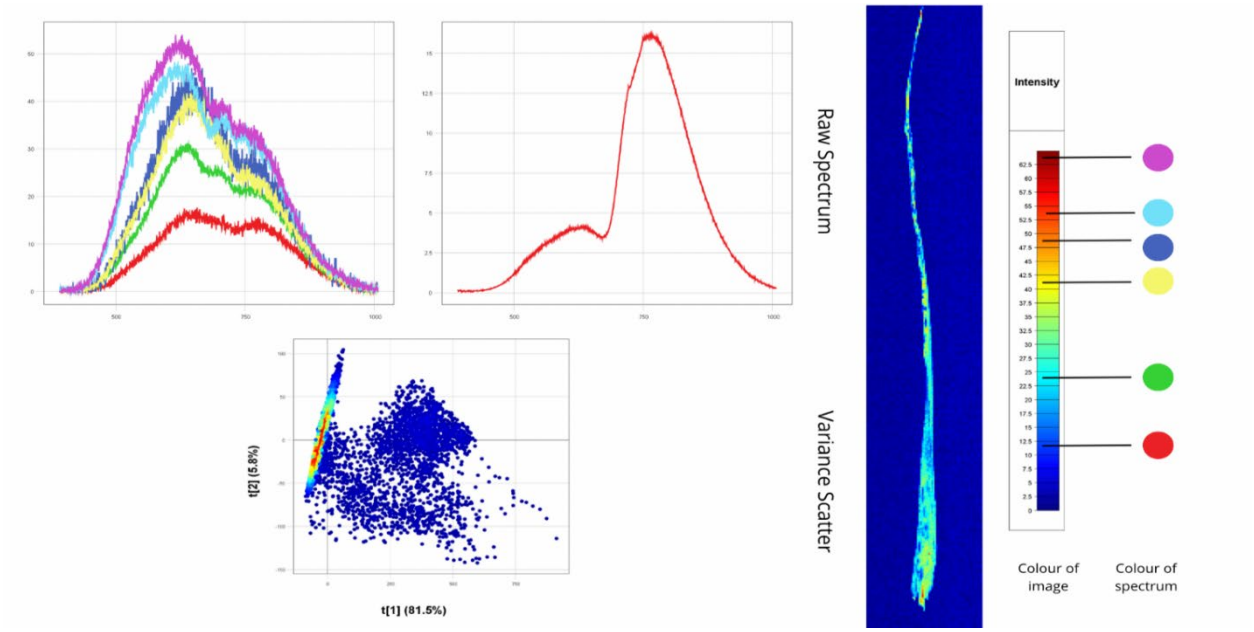

Note: Compiled by the author

Figure 13
Sample K: Leaf spot

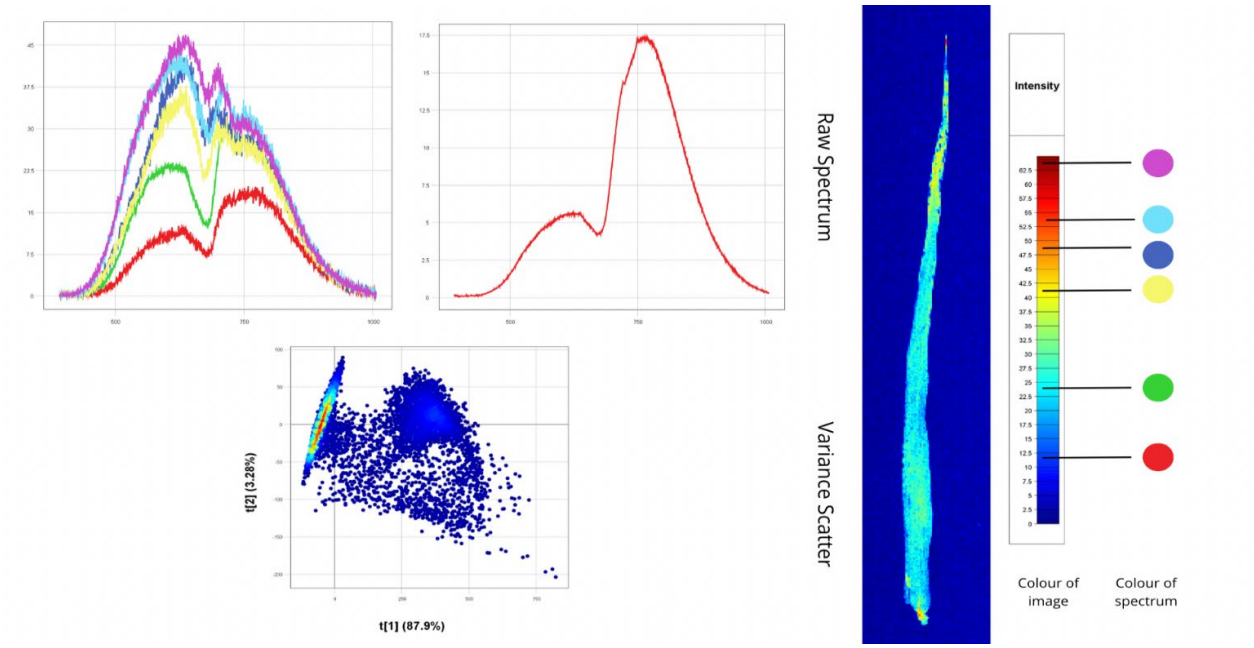

Note: Compiled by the author

Figure 14 presents a hyperspectral image of three barley leaves affected by leaf spot. Examining the colour expression of individual areas, it can be noted that regions coloured dark blue correspond to low reflectance intensity, which may indicate necrosis or other tissue damage. Areas coloured yellow and light blue have medium intensity and belong to affected zones where leaf spot is not pronounced. In the Raw Spectrum graphs, the purple curve corresponds to areas with maximum reflectance, correlating with potentially healthy tissues. Meanwhile, in the graph of the leaves' overall spectra, the first sample is characterised by the lowest intensity of all, as it contains more affected tissue, while the third sample has the highest reflectance coefficient, as it contains unaffected (i.e., healthy) plant tissues. The Variance Scatter graph clearly displays the result of the Principal Component Analysis (PCA), where the t[1] axis (82.4%) represents the main component explaining the primary data variability, and the t[2] axis (8.45%) represents the second component. Each point in this case represents a spectrum from a specific image pixel, and its colour, in turn, reflects the colour of the corresponding spectrum.

Figure 14
Sample J: Leaf spot

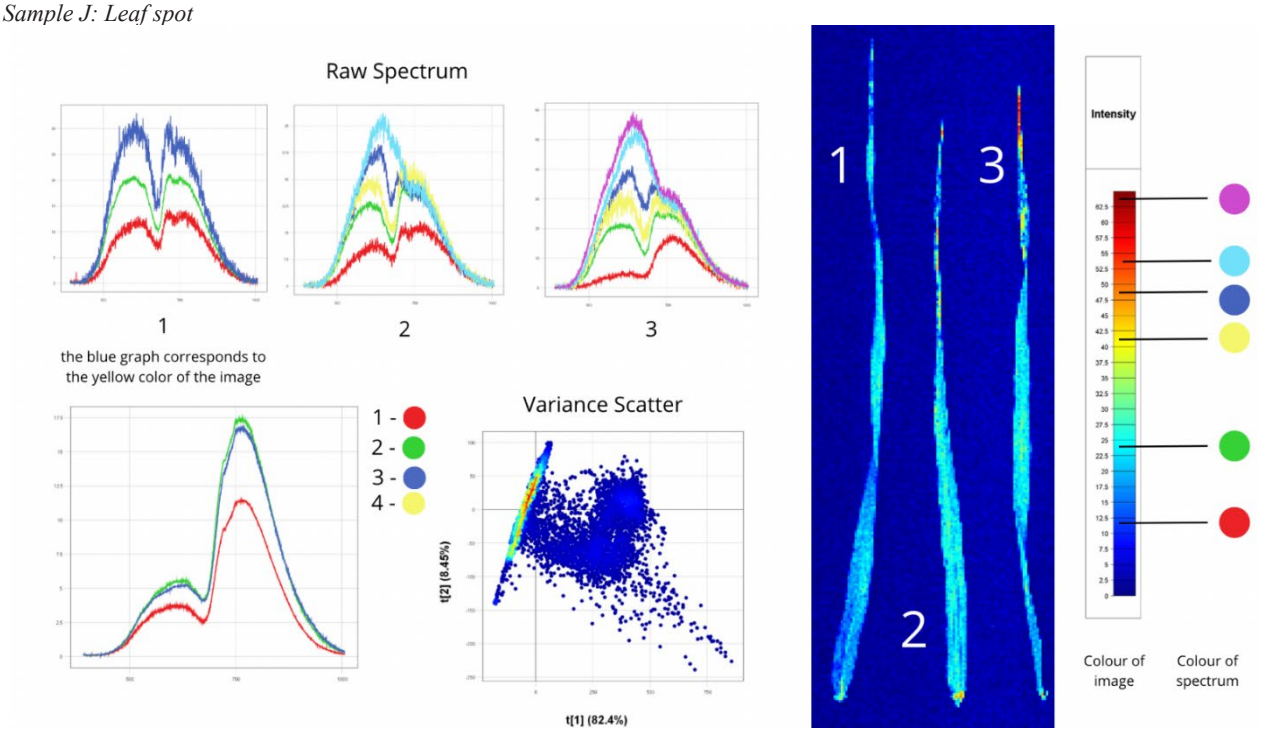

Note: Compiled by the author

Figure 15 clearly shows areas on barley leaves affected by leaf spot. Their manifestation is visualised as dark blue spots, mainly concentrated in the central part. These areas correspond to minimal reflectance intensity (typically recorded in the range of 7.5-10), which appears in varied colouration: for example, areas with the initial stage of leaf spot are coloured yellow and light blue and have medium spectral intensity, while healthy leaf zones are displayed in red and have high reflectance. Despite the plant containing healthy tissues, the overall reflectance is usually low, which may be a result of the evident disease infection. The overall spectral profile is characterised by a distinct peak in the approximate range of 700 to 800 nm.

Figure 15
Sample L: Leaf spot

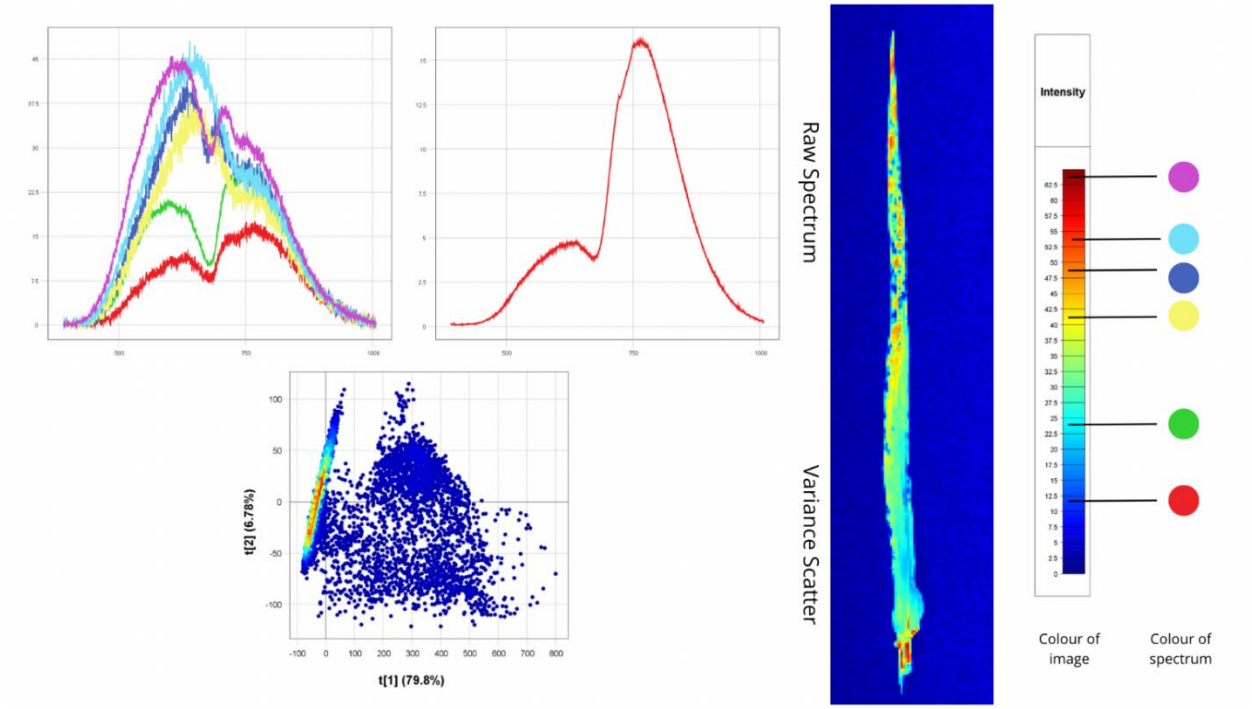

Note: Compiled by the author

Root rot

Figure 16 shows that the roots of all samples in the hyperspectral image are coloured blue, indicating infection with root rot. The first sample contains the fewest light areas along its entire length, which may indicate that its spectrum has the lowest intensity. The third sample, in turn, contains the greatest amount of healthy tissue, meaning its roots are less affected by the disease than the others; therefore, its spectrum has the highest intensity. Consequently, on the Variance Scatter diagram, the t[1] axis (86.3%) reflects the main share of variation (almost 90%) in terms of spectral data, while the t[2] axis (8.3%) captures additional differences.

Figure 17 depicts two plant roots affected by root rot. In the Raw Spectrum graphs, the spectra of infected zones (red curve) have low values – typically around 11. In the hyperspectral image itself, they are displayed in blue, while in the overall graph, the second sample has a higher reflectance coefficient than the first, as it contains more areas with healthy tissue.

Figure 18 shows a single plant with signs of root rot on the roots. In the hyperspectral image, healthy and infected root sections can be clearly distinguished. It was established that healthy tissues correspond to red zones in the image, while areas of the root affected by rot are displayed in blue and light blue. This colour manifestation is particularly noticeable closer to the lower root branches. Analysis of the Raw Spectrum graphs shows characteristic peaks of reflected light intensity in different spectral ranges. The purple curve on the first graph represents healthy plant tissues and has a high reflectance value- approximately within 80 units – while infected tissues have significantly lower reflectance, most often not exceeding 18.

Figure 16
Sample M: Root rot

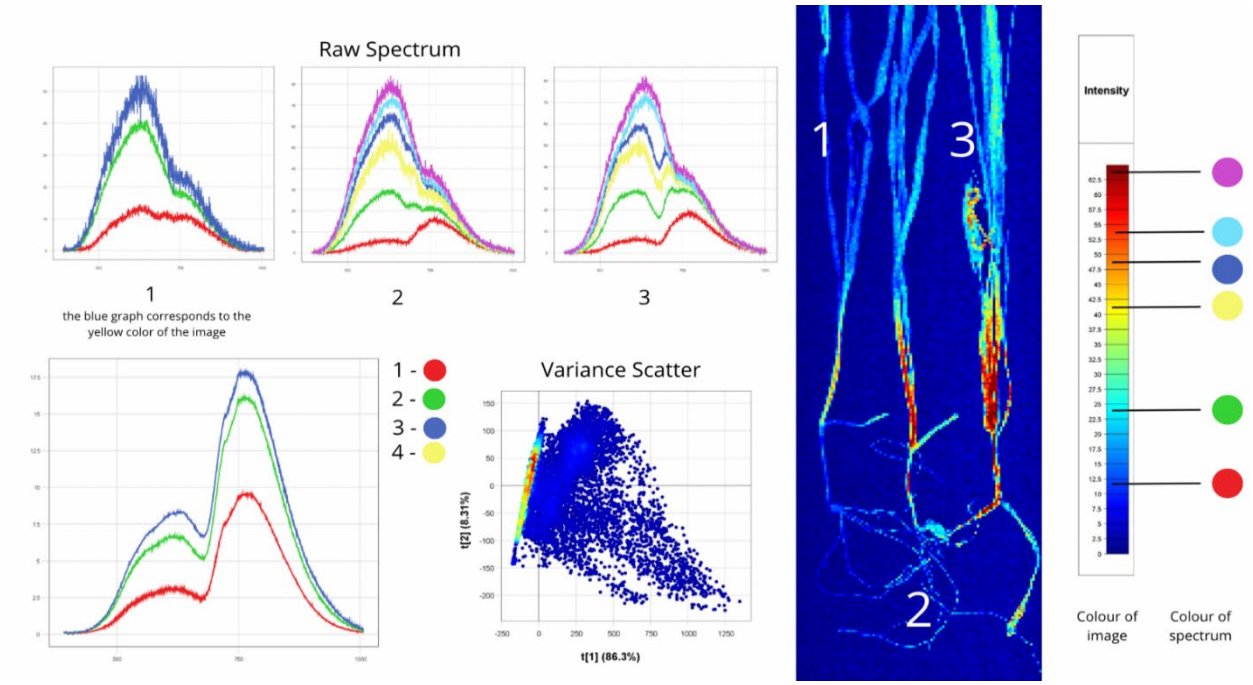

Note: Compiled by the author

Figure 17
Sample N: Root rot

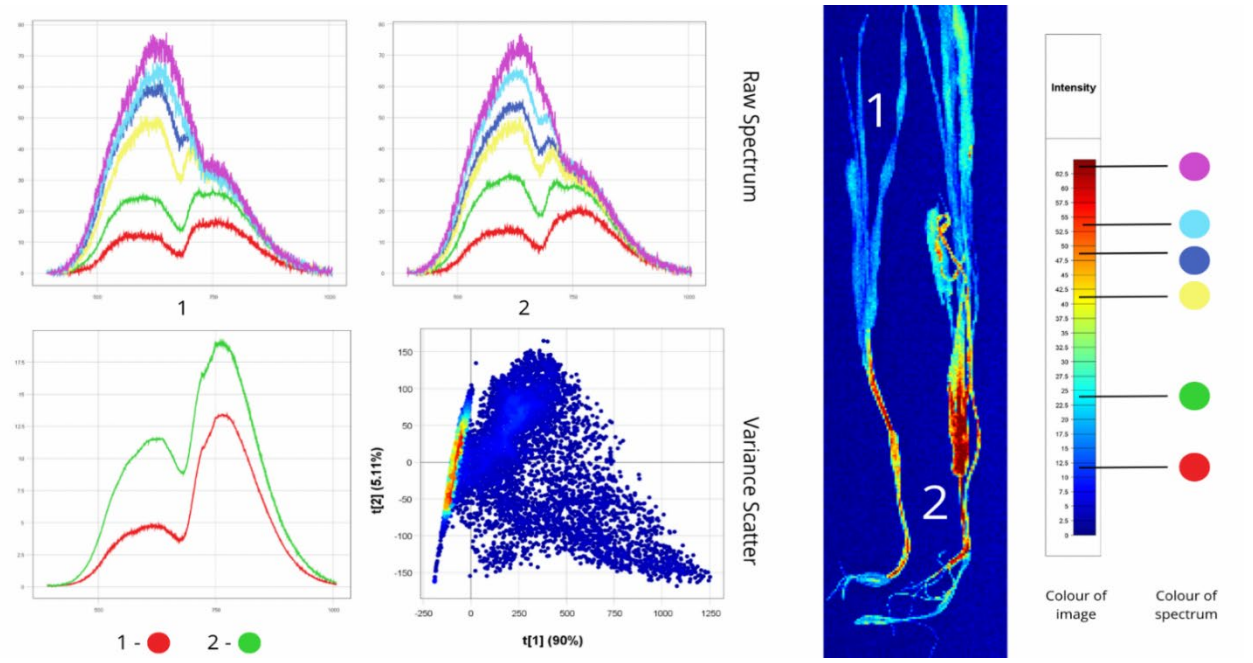

Note: Compiled by the author

Figure 18
Sample O: Root rot

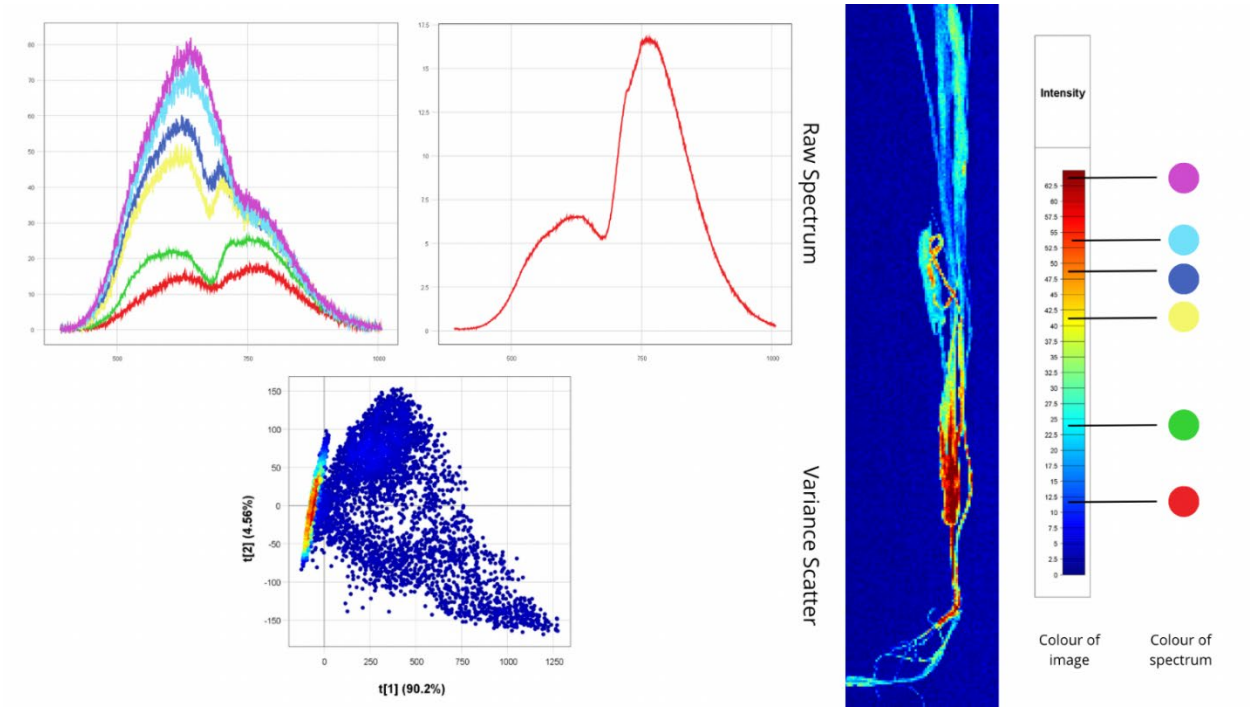

Note: Compiled by the author

Thus, it was found that, in general, the overall spectrum of a diseased plant has a maximum reflectance coefficient of 18, while the overall spectrum of a healthy plant is characterised by a reflectance coefficient around 30. Summarised data on spectral characteristics are presented in Table 1.

Table 1
Spectral characteristics of barley

№	Type	Sample	Wavelength (nm)	Spectral reflectance (%)
1	Healthy		550-750	15-45
2	Loose smut	Sample A	500-780	10-18
		Sample B	500-780	10-18
		Sample C	500-750	8-20
		Sample D	500-780	8-21
		Sample E	500-800	10-20
3	Leaf spot	Sample G	500-800	4-23
		Sample I	500-780	13-30
		Sample J	500-780	5-30
		Sample K	600-780	11-30
		Sample L	500-800	11-26
4	Plant rust	Sample H	500-780	12-19
		Sample P	550-780	15-21
5	Root rot	Sample M	500-800	6-20
		Sample N	500-800	12-21
		Sample O	550-800	15-19

Note: Compiled by the author

For an objective interpretation of the obtained hyperspectral data, comprehensive statistical processing is required to identify patterns, quantitative differences, and statistically significant features of barley's reflective characteristics. Hyperspectral imaging generates a large volume of multidimensional data, necessitating the application of mathematical statistics methods for organisation, summarisation, and interpretation.

The statistical analysis in this study aimed to assess the distribution of spectral indicators and identify variability in reflectance at different wavelengths. Tables 2 and 3 present these statistical data for reflectance coefficient and wavelength, visualised in graphs in Images 19 and 20 using VisualizeFree.

The highest maximum reflectance is observed in the healthy sample due to the reflectance of healthy tissue saturated with the green pigment chlorophyll; the lowest is in leaf spot due to the low reflectance of dark, necrotic plant tissue. The mean reflectance value simplifies complex spectral data into a single numerical indicator, facilitating comparison between diseases. It was determined that samples with loose smut have the lowest mean value, as the disease is characterised by dark-coloured lesions reflecting little light. The highest mean among diseases was found in samples with initial stages of leaf spot, which has not yet progressed to necrosis and exhibits a yellow colour. The highest mean reflectance overall belongs to the healthy barley sample.

Table 2
Statistical indicators of reflectance and wavelengths

Type	Sample	Spectral reflectance (%)							Wavelength (nm)			
		Min Reflectance	Max Reflectance	Mean Reflectance	Standard Deviation	CV	Median	Delta Reflectance	Min	Max	Spectral Bandwidth	Spectral Skewness
Healthy		15	45	27.50	8.66	31.49	27.50	30	550	750	200	0.5
Loose smut	Sample A	10	18	14.00	2.31	16.50	14.00	8	500	780	280	0
	Sample B	5	18	12.00	3.75	31.27	12.00	13	500	780	280	-0.22
	Sample C	8	20	14.00	3.46	24.74	14.00	12	500	750	250	0
	Sample D	8	21	14.75	3.75	25.44	14.75	13	500	780	280	-0.03
	Sample E	10	20	15.00	2.89	19.25	15.00	10	500	800	300	0
Leaf spot	Sample G	4	23	15.50	5.48	35.39	15.50	19	500	800	300	-0.74
	Sample I	13	30	20.00	4.91	24.54	20.00	17	500	780	280	0.45
	Sample J	5	30	18.00	7.22	40.09	18.00	25	500	780	280	-0.16
	Sample K	11	30	20.75	5.48	26.43	20.75	19	500	780	280	-0.1
	Sample L	11	26	18.50	4.33	23.41	18.50	15	500	800	300	0
Plant rust	Sample H	12	19	15.25	2.02	13.25	15.25	7	500	780	280	0.24
	Sample P	15	21	18.00	1.73	9.62	18.00	6	470	780	310	0
Root rot	Sample M	6	20	14.00	4.04	28.87	14.00	14	500	800	300	-0.37
	Sample N	12	21	16.00	2.60	16.24	16.00	9	500	800	300	0.21
	Sample O	15	19	17.00	1.15	6.79	17.00	4	490	800	310	0

Note: Compiled by the author

Analysis of standard deviation helps assess the stability, predictability, and homogeneity of data in the study. The standard deviation values among the presented samples are low, confirming measurement reproducibility for each disease. For example, for sample O, $\sigma = 1.15\%$, meaning most values lie within ±1.15% of the mean. It was noted that the healthy barley sample exhibits moderate variability in the coefficient of variation, as healthy plant tissue has different reflectance depending on the area and the percentage of chlorophyll in the tissues. The

study of the reflectance of various plant parts affected to different degrees by barley disease pathogens showed that:

- samples with loose smut and root rot have low to medium values, depending on the degree of plant infection;

- samples with leaf spot have the highest values of the coefficient of variation, as different disease stages are characterised by varying degrees of reflectance;

- samples affected by rust have the lowest values, indicating data homogeneity and low disease variability.

Figure 19
Visualisation of reflectance coefficient statistics

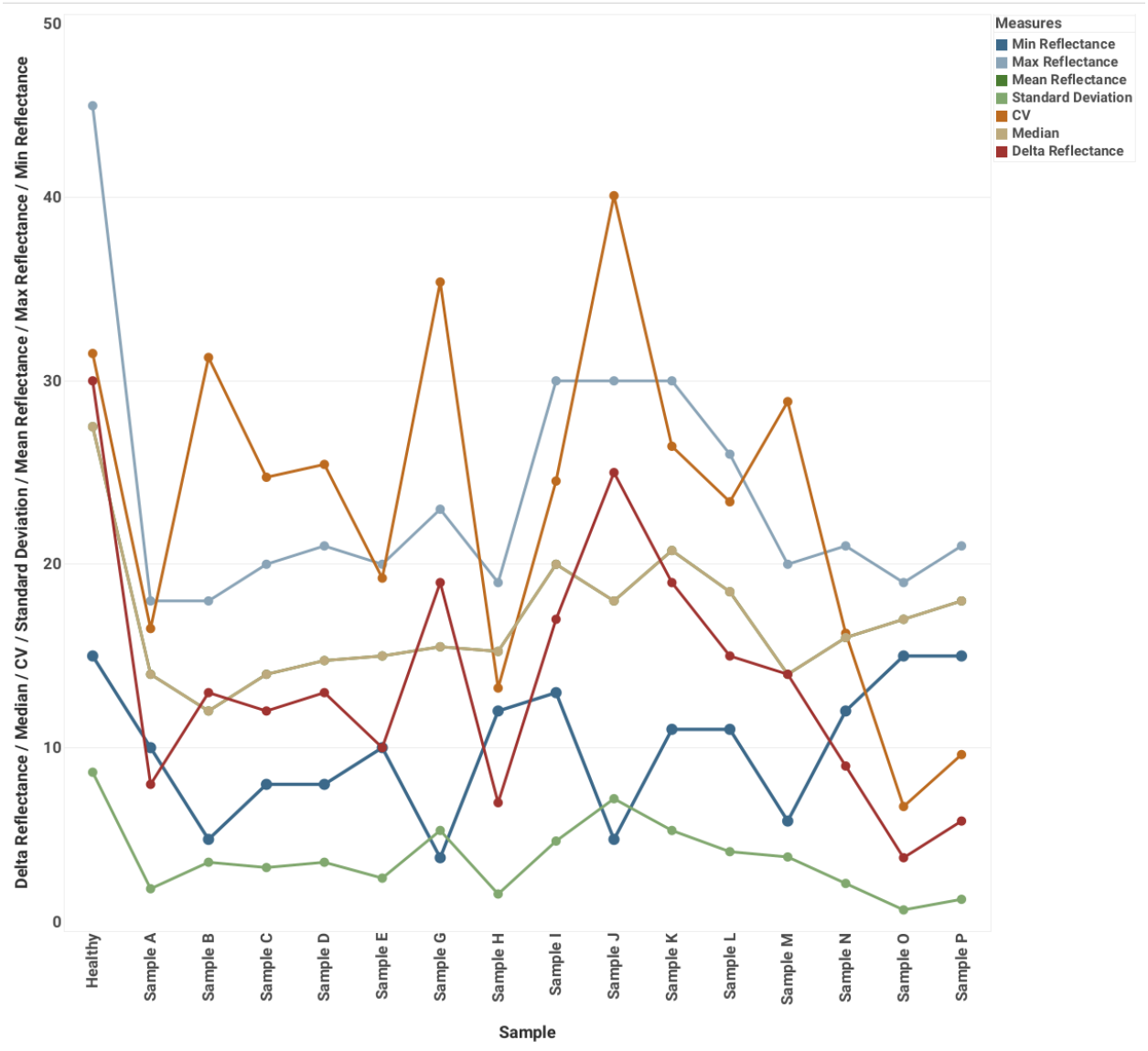

Note: Compiled by the author

Among all samples studied during the laboratory research, the highest value of reflectance delta is observed in healthy tissues, associated with varying chlorophyll content and, consequently, different reflectance of plant areas. Among diseases, the highest reflectance deltas are observed in samples with leaf spot due to different stages of leaf infection, where initial stages have

a higher reflectance coefficient than those characteristic of necrosis stages. The most stable indicators were found in samples with rust and root rot.

The healthy sample registers the narrowest range, as reflectance is concentrated in the photosynthetically active radiation (PAR) region. A narrow reflectance spectrum may indicate stable leaf structure and sufficient chlorophyll content, resulting in uniform energy reflectance. It was established that the spectral range widens in damaged or altered tissues. An increase in spectral bandwidth is observed primarily in diseased samples, indicating changes in pigment and tissue structure. It is also important to note the appearance of reflectance scattering at additional wavelengths, which is presumably associated with partial cell destruction and the emergence of atypical optical properties. Leaf spot leads to plant deterioration and causes mosaic tissue damage, where some areas are healthy and others are necrotic. Obviously, loose smut, rust, and root rot have pigmentations different from healthy tissue; therefore, the changes induced by these diseases broaden the spectral range.

This leads to the possibility of determining that the highest value of the spectral band is mainly observed in samples with root rot. An important indicator, alongside those mentioned above, is spectral skewness. Skewness values greater than zero generally indicate a healthy overall plant condition, chlorophyll accumulation, and an active photosynthetic zone noted in the 700-800 nm range. It was noted that the identified spectral limit shifts to the left in the presence of damaged or degraded tissues, which is usually associated with reduced chlorophyll levels in these areas and a predominance of reflectance at shorter wavelengths. Such spectral skewness is often present precisely in diseased samples, which may serve as evidence of their pathogenic vulnerability.

Figure 20
Visualisation of statistical wavelength data

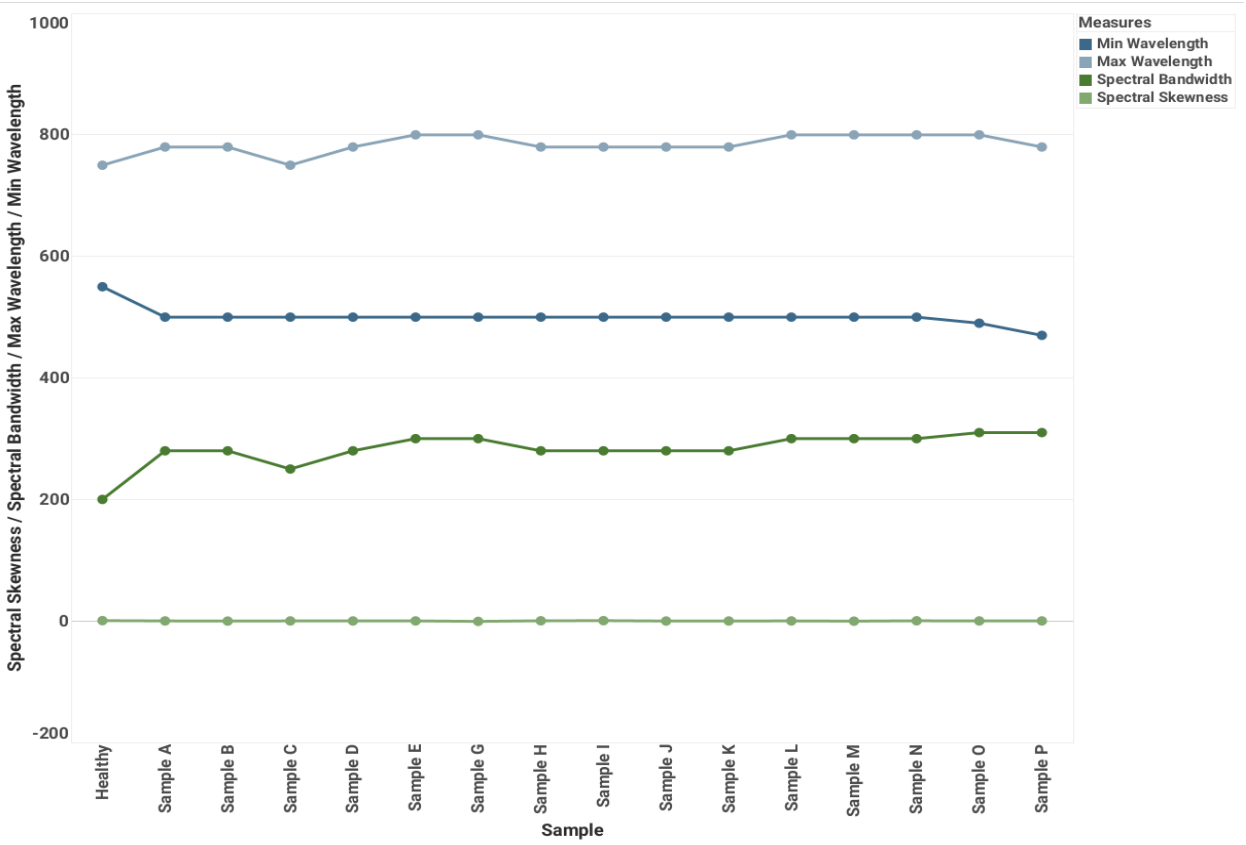

Note: Compiled by the author

Hyperspectral visualisation can identify pathogens and determine their molecular structure. The dark colour of fungal plant diseases may be due to adaptation for spore dispersal and survival in field conditions. While there is no comprehensive scientific data on melanin content in loose smut to date, the dark colour may be due to the presence of this pigment, as in *Podospora anserina* (Gautier et al., 2021), *Pestalotiopsis microspora* (Yu et al., 2015), and *Ustilago maydis* (Reyes-Fernández et al., 2021). Melanin can protect fungal spores from UV radiation, increase resistance to desiccation, and thicken spore cell walls; due to its dark colour, loose smut absorbs more light than it reflects, so the spectra of plant parts affected by fungi will be sharply distinguished by reduced intensity. Plant rust is caused by the fungus *Puccinia graminis*, which typically spreads spores with melanin-like pigments. Urediniospores contain flavonoid derivatives and carotenoids, such as β-carotene and γ-carotene (Davoli et al., 2002), which protect spores from UV radiation and oxidative processes and impart a rusty colour. Teliospores, in turn, may contain melanin-like pigments, as genes encoding laccase-like proteins (Tao et al., 2017) and laccase enzymes (Zhan et al., 2023) have been identified in rust-causing fungi, which is why rust can appear brown or dark. The principle and possibility of differentiating these lesions from other diseases are interesting, manifested as separately located blue areas in the hyperspectral image. Regarding root rot, it was found to have dark pigments, making it noticeable by low spectral intensity in the root area. Dark pigments may help pathogenic fungi cause rot, as in the case of white rot (Lujan et al., 2016), promote fungal survival in soil as with black root rot (Netherway et al., 2024), and possess toxicity. Research on enhanced melanin production in studies within this thematic area allowed the authors to establish that the obtained results correlate with an increase in the number of fungal genomes in wheat roots and an intensification of disease symptoms (Aranda et al., 2023; Henson et al., 1999). It was also established that leaf spot in the initial stage, during chlorophyll destruction, has a yellow colour that can be confused with healthy plant tissue; however, with the accumulation of metabolites and necrosis, pigmented spots of brown and dark colours appear. It was determined that in hyperspectral imaging, leaf spot can be differentiated by the presence of blue dots on leaf tips.

Image 21 presents a combined comparative graph of reflectance spectra. The spectrum of the healthy plant shows the highest reflectance. The spectrum of leaf spot has the highest reflectance among all diseases due to disease variability, while the spectrum of loose smut is characterised by the lowest intensity.

Image 22 demonstrates the difference in spectra between a healthy and a diseased plant.

Figure 21
Comparative graph of reflectance spectra

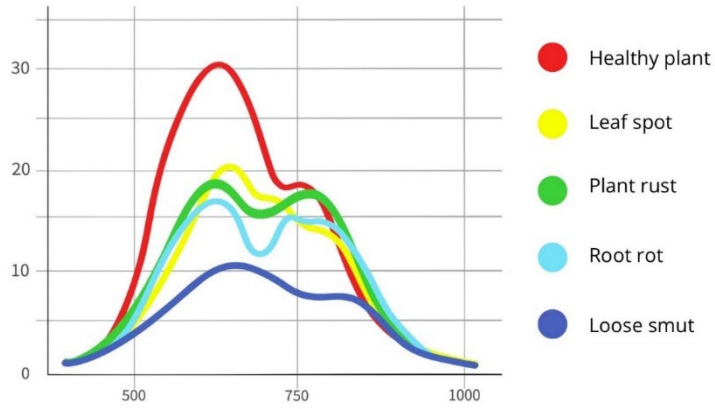

Note: Compiled by the author

Figure 22
A comparative image reflecting the difference between a healthy and a diseased plant

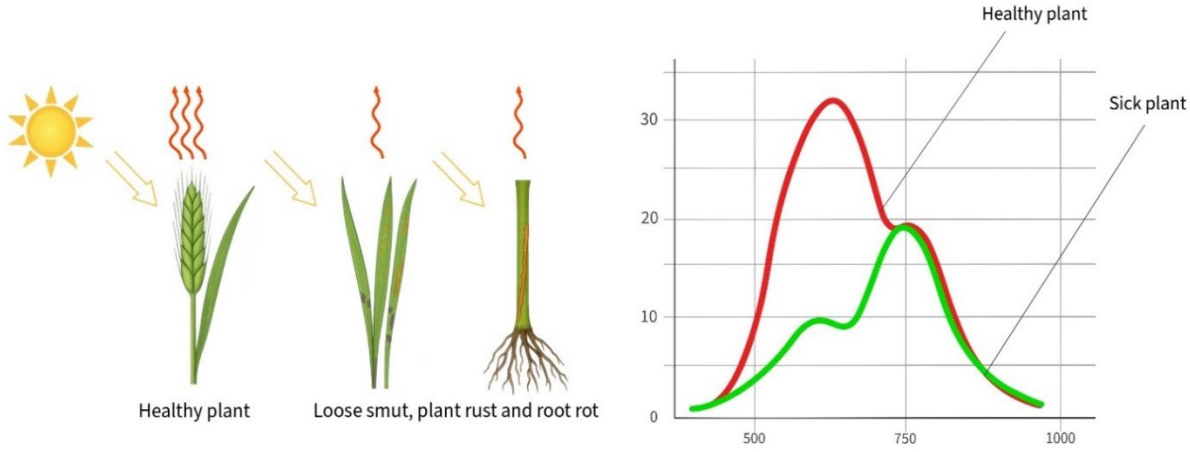

Note: Compiled by the author

The conducted research clearly shows that healthy plant tissue has a high reflectance coefficient due to the green pigment chlorophyll and the white areas of the root base. This is because chlorophyll actively absorbs light in the blue and red ranges (400-500 nm and 600-700 nm) and reflects well in the green range of the visible spectrum (500-600 nm), as well as in the near-infrared range (from 700 nm). It was also established that in the near-infrared range (700-800 nm), chlorophyll does not absorb light, so most of the radiation is reflected by leaf tissues. Moreover, in diseased plants, reflectance decreases across the entire range due to disruption of the overall epidermis structure, darkening of areas, destruction of mesophyll, suppression of chlorophyll synthesis, and lack of photosynthetic activity, which blocks light reflectance.

In general, hyperspectral visualisation allows for the differentiation of healthy and infected barley samples. A healthy plant demonstrates a high level of reflectance, while infected samples are characterised by reduced reflectance and increased spectral variability. It is important to note that the severity of these changes depends on the nature and localisation of the disease: for example, loose smut, rust, and root rot cause systemic disorders, leading to a sharp decrease in reflectance and tissue degradation. Leaf spot, on the other hand, forms a mosaic structure in the late stages of the disease, manifested in high spectral heterogeneity and variability.

Thus, hyperspectral imaging serves as an effective tool for early and non-destructive detection of phytopathological conditions, enabling precise monitoring of plant physiological status and prompt response to threats in agrocenosis.

Conclusion

One of the main challenges in agriculture is the inability to achieve early disease diagnosis. Plant infections often remain undetected for long periods, as the parasite's mycelium spreads diffusely within the host plant without causing external changes. In this context, hyperspectral imaging enables disease identification at early stages, preventing its further spread. By studying the spectral characteristics of barley diseases such as loose smut, leaf spot, and root rot, it was revealed that plant areas infected or desiccated have a low reflectance coefficient, initial disease stages have a medium coefficient, and healthy tissue exhibits high spectral intensity.

In hyperspectral images, diseased plant areas are displayed in blue, areas with still-living but already infected tissue appear in yellow, while healthy plant areas are shown in orange, red, and burgundy. It was found that spectra from healthy areas possess high intensity compared to spectra from disease-affected

zones. This is because healthy tissue contains the green pigment chlorophyll, which actively reflects light. The destruction of the epidermis structure, loss of moisture, tissue necrosis, and darkening lead to a pronounced decrease in reflected light intensity. Barley diseases like loose smut, rust, and root rot contain spores with melanin-like pigments. These cause the decay of healthy tissues, suppress the activity of photosynthetic systems, and absorb more light than they reflect. It becomes evident that these diseases can be primarily identified by the reduced reflectance coefficient of infected plant parts. The study of leaf spot at its initial stage showed that during chlorophyll destruction, these lesions exhibit a yellow colour, which can be mistaken for healthy plant tissue. As metabolites accumulate and necrosis develops, pigmented spots of brown and dark colours appear, resulting in high variability in the spectra of this disease. It was established that leaf spot can be differentiated by the non-uniform intensity of spectra detected across different parts of the plant; consequently, a distinguishing feature of all phytopathologies can be considered the overall reduction in the plant's reflective capacity.

The obtained data on barley's spectral profiles position hyperspectral imaging as a method for monitoring barley agrocenoses. It enables the differentiation of phytopathologies, detailed analysis of crop conditions at the level of individual plants, and the detection of anomalies before the manifestation of external symptoms. Further developments in this area will allow for targeted application of protective agents, reduced pesticide expenditures, and decreased environmental impact. Thus, hyperspectral imaging represents a crucial tool for precision agriculture, aimed at the sustainable and efficient management of barley crops.

Funding

This research is funded by the Science Committee of the Ministry of Science and Higher Education of the Republic of Kazakhstan (Grant No. AP23485162 “Development of an innovative method for monitoring and early diagnosis of grain crop diseases using hyperspectral sensing technology”).

Author contribution

The manuscript was written through contributions of all authors. All authors have given approval to the final version of the manuscript: Conceptualisation, Ualiyeva R.M.; Methodology, Diyanchuk N.A.; Software, Kaverina M.M.; Formal Analysis, Diyanchuk N.A.; Investigation, Kaverina M.M.; Resources, Zhangazin S.B.; Data Curation, Zhangazin S.B.; Writing – Original Draft Preparation, Osipova A.V.; Writing – Review & Editing, Tuyakbayeva A.U.; Visualisation, Osipova A.V.; Supervision, Ualiyeva R.M.; Project Administration, Tuyakbayeva A.U.; Funding Acquisition, Ualiyeva R.M.

References

Thomas, S., Behmann, J., Steier, A., et al. (2018). Quantitative assessment of disease severity and rating of barley cultivars based on hyperspectral imaging in a non-invasive, automated phenotyping platform. *Plant Methods*, 14, 45. https://doi.org/10.1186/s13007-018-0313-8

Zhou, R.-Q., Jin, J.-J., Li, Q.-M., Su, Z.-Z., Yu, X.-J., Tang, Y., Luo, S.-M., He, Y., & Li, X.-L. (2019). Early detection of Magnaporthe oryzae-infected barley leaves and lesion visualization based on hyperspectral imaging. *Frontiers in Plant Science*, 9, 1962. https://doi.org/10.3389/fpls.2018.01962

Senthilkumar, T., Jayas, D. S., White, N. D. G., Fields, P. G., & Gräfenhan, T. (2016). Detection of fungal infection and ochratoxin A contamination in stored barley using near-infrared hyperspectral imaging. *Biosystems Engineering*, 147, 162-173. https://doi.org/10.1016/j.biosystemseng.2016.03.010

Kuska, M. T., Brugger, A., Thomas, S., Wahabzada, M., Kersting, K., Oerke, E.-C., Steiner, U., & Mahlein, A.-K. (2017). Spectral patterns reveal early resistance reactions of barley against *Blumeria graminis f. sp. hordei*. *Phytopathology*, 107(11), 1388–1398. https://doi.org/10.1094/PHYTO-04-17-0128-R

Kuśka, M. T. (2017). *Hyperspectral imaging for non-invasive characterization of barley resistances to powdery mildew* (Doctoral dissertation). Rheinische Friedrich-Wilhelms-Universität Bonn, Universitäts- und Landesbibliothek Bonn. URN: urn:nbn:de:hbz:5n-49015

Yu, K., Leufen, G., Hunsche, M., Noga, G., Chen, X., & Bareth, G. (2014). Investigation of leaf diseases and estimation of chlorophyll concentration in seven barley varieties using fluorescence and hyperspectral indices. *Remote Sensing*, 6(1), 64-86. https://doi.org/10.3390/rs6010064

Su, W.-H., Yang, C., Dong, Y., Johnson, R., Page, R., Szinyei, T., Hirsch, C. D., & Steffenson, B. J. (2021). Hyperspectral imaging and improved feature variable selection for automated determination of deoxynivalenol in various genetic lines of barley kernels for resistance screening. *Food Chemistry*, 343, 128507. https://doi.org/10.1016/j.foodchem.2020.128507

Brugger, A., Schramowski, P., Paulus, S., Steiner, U., Kersting, K., & Mahlein, A.-K. (2021). Spectral signatures in the UV range can be combined with secondary plant metabolites by deep learning to characterize barley–powdery mildew interaction. *Plant Pathology*, 70(7), 1572-1582. https://doi.org/10.1111/ppa.13411

Kuska, M., Wahabzada, M., Leucker, M., Dehne, H.-W., Kersting, K., Oerke, E.-C., Steiner, U., & Mahlein, A.-K. (2015). Hyperspectral phenotyping on the microscopic scale: Towards automated characterization of plant-pathogen interactions. *Plant Methods*, 11, 28. https://doi.org/10.1186/s13007-015-0073-7

Thomas, S., Wahabzada, M., Kuska, M. T., Rascher, U., & Mahlein, A.-K. (2016). Observation of plant–pathogen interaction by simultaneous hyperspectral imaging reflectance and transmission measurements. *Functional Plant Biology*, 44(1), 23-34. https://doi.org/10.1071/FP16127

State Standard 12044-93. (2011). *Methods for Determining Disease Contamination*. Standartinform: Moscow. p. 57.

Ualiyeva, R. M., Kaverina, M. M., Osipova, A. V., Kairbayev, Y. B., Zhangazin, S. B., Iksat, N. N., & Mapitov, N. B. (2025). VNIR hyperspectral signatures for early detection and machine-learning classification of wheat diseases. *Plants*, 14(23), 3644. https://doi.org/10.3390/plants14233644

Gautier, V., Levert, E., Giraud, T., & Silar, P. (2021). Important role of melanin for fertility in the fungus *Podospora anserina. G3: Genes | Genomes | Genetics*, 11(8). https://doi.org/10.1093/g3journal/jkab159

Yu, X., Huo, L., Liu, H., Chen, L., Wang, Y., & Zhu, X. (2015). Melanin is required for the formation of the multi-cellular conidia in the endophytic fungus *Pestalotiopsis microspora*. *Microbiological Research*, 179, 1-11.

Reyes-Fernández, E. Z., Shi, Y.-M., & Grün, P. (2021). An unconventional melanin biosynthesis pathway in *Ustilago maydis*. *Applied and Environmental Microbiology*. https://doi.org/10.1128/AEM.01510-20

Davoli, P., & Weber, R. W. (2002). Identification and quantification of carotenoid pigments in aeciospores of the daisy rust fungus *Puccinia distincta*. *Phytochemistry*, 60(3), 309-313. https://doi.org/10.1016/S0031-9422(02)00120-6

Tao, S. Q., Cao, B., Tian, C. M., et al. (2017). Comparative transcriptome analysis and identification of candidate effectors in two related rust species (*Gymnosporangium yamadae* and *Gymnosporangium asiaticum*). *BMC Genomics*, 18, 651. https://doi.org/10.1186/s12864-017-4059-x

Zhan, G., Guo, J., Tian, Y., et al. (2023). High-throughput RNA sequencing reveals differences between the transcriptomes of the five spore forms of *Puccinia striiformis f. sp. tritici*, the wheat stripe rust pathogen. *Stress Biology*, 3, 29. https://doi.org/10.1007/s44154-023-00107-z

Lujan, P., Sanogo, S., & Puppala, N. (2016). Factors affecting mycelium pigmentation and pathogenicity of *Sclerotinia sclerotiorum* on Valencia peanut. *Canadian Journal of Plant Science*. https://doi.org/10.1139/cjps-2015-0258

Netherway, T., Bengtsson, J., Buegger, F., Fritscher, J., Oja, J., Pritsch, K., Hildebrand, F., Krab, E. J., & Bahram, M. (2024). Pervasive associations between dark septate endophytic fungi with tree root and soil microbiomes across Europe. *Nature Communications*, 15, 159. https://doi.org/10.1038/s41467-023-44172-4

Aranda, C., Méndez, I., & Barra, P. J. (2023). Melanin induction restores the pathogenicity of *Gaeumannomyces graminis* var. tritici in wheat plants. *Journal of Fungi*, 9(3), 350. https://doi.org/10.3390/jof9030350

Henson, J. M., Butler, M. J., & Day, A. W. (1999). The dark side of the mycelium: Melanins of phytopathogenic fungi. *Annual Review of Phytopathology*, 37, 447-471. https://doi.org/10.1146/annurev.phyto.37.1.447

Information about authors:

Ualiyeva Rimma Meyramovna (corresponding author) – PhD, Professor of the Department of Biology and Ecology, Toraighyrov University (Pavlodar, Kazakhstan, e-mail: ualiyeva.r@gmail.com).

Osipova Anastasiya Vyacheslavovna – Master's degree student, Department of Biology and Ecology, Toraighyrov University (Pavlodar, Kazakhstan, e-mail: aanastasiyaaa@internet.ru).

Diyanchuk Nikita Aleksandrovich – Bachelor's degree student, Department of Biology and Ecology, Toraighyrov University (Pavlodar, Kazakhstan, e-mail: nik.diyanchuk@gmail.com).

Kaverina Mariya Mikhailovna – Master of Natural Sciences, Junior Researcher at the Department of Biology and Ecology, Toraighyrov University (Pavlodar, Kazakhstan, e-mail: k.ma96@mail.ru).

Zhangazin Sayan Berikovich – PhD, Associate Professor, Acting Deputy Director for Research at the Institute of Natural Sciences, L.N. Gumilyov Eurasian National University (Astana, Kazakhstan, e-mail: sayanzhangazin@gmail.com).

Tuyakbayeva Akmaral Userkhanovna – Candidate of Biological Sciences, Associate Professor of the Department of Biotechnology and Microbiology, L.N. Gumilyov Eurasian National University (Astana, Kazakhstan, e-mail: akmaral.t@inbox.ru).

Авторлар туралы мәлімет:

Уалиева Римма Мейрамовна (корреспонденттік автор) – PhD, «Биология және экология» кафедрасының профессоры, Торайғыров университеті (Павлодар, Қазақстан, e-mail: ualiyeva.r@gmail.com).

Осипова Анастасия Вячеславовна – магистрант, «Биология және экология» кафедрасы, Торайғыров университеті (Павлодар, Қазақстан, e-mail: aanastasiyaaa@internet.ru).

Диянчук Никита Александрович – бакалавриат студенті, «Биология және экология» кафедрасы, Торайғыров университеті (Павлодар, Қазақстан, e-mail: nik.diyanchuk@gmail.com).

Каверина Мария Михайловна – жаратылыстану ғылымдарының магистрі, «Биология және экология» кафедрасының кіші ғылыми қызметкері, Торайғыров университеті (Павлодар, Қазақстан, e-mail: k.ma96@mail.ru).

Жангазин Саян Берикович – PhD, қауымдастырылған профессор, Жаратылыстану ғылымдары институты директорының ғылыми жұмыс жөніндегі орынбасары м.а., Л.Н. Гумилев атындағы Еуразия ұлттық университеті (Астана, Қазақстан, e-mail: sayanzhangazin@gmail.com).

Туякбаева Акмарал Усерхановна – биология ғылымдарының кандидаты, «Биотехнология және микробиология» кафедрасының қауымдастырылған профессоры, Л.Н. Гумилев атындағы Еуразия ұлттық университеті (Астана, Қазақстан, e-mail: akmaral.t@inbox.ru).

Сведения об авторах:

Уалиева Римма Мейрамовна (автор-корреспондент) – PhD, профессор кафедры «Биология и экология», Торайгыров университет (Павлодар, Казахстан, e-mail: ualiyeva.r@gmail.com).

Осипова Анастасия Вячеславовна – магистрант, кафедра «Биология и экология» Торайгыров университета (Павлодар, Казахстан, e-mail: aanastasiyaaa@internet.ru).

Диянчук Никита Александрович – студент бакалавриата, кафедра «Биология и экология», Торайгыров университет (Павлодар, Казахстан, e-mail: nik.diyanchuk@gmail.com).

Каверина Мария Михайловна – магистр естественных наук, младший научный сотрудник кафедры «Биология и экология», Торайгыров университет (Павлодар, Казахстан, e-mail: k.ma96@mail.ru).

Жангазин Саян Берикович – PhD, ассоциированный профессор, и.о. заместителя директора по научной работе института Естественных наук, Евразийский национальный университет имени Л.Н. Гумилева (Астана, Казахстан, e-mail: sayanzhangazin@gmail.com).

Туякбаева Акмарал Усерхановна – кандидат биологических наук, ассоциированный профессор кафедры «Биотехнология и микробиология», Евразийский национальный университет имени Л.Н. Гумилева (Астана, Казахстан, e-mail: akmaral.t@inbox.ru).

Received December 22, 2025
Accepted June 15, 2026